ISRN LUTMDN/TMHP—10/5229—SE
ISSN 0282-1990

Large Eddy Simulations of Wind Turbines Employing the Virtual Boundary Method

Sten Edström Barup

Thesis for the Degree of Master of Science

Division of Fluid Mechanics
Department of Energy Sciences
Faculty of Engineering
Lund University

Large Eddy Simulations of Wind Turbines Employing the Virtual Boundary Method

– *a study on the influence of pitch control on wake interaction*

by
Sten Edström Barup

supervisor
Robert-Zoltán Szász

A thesis submitted to the
Faculty of Engineering
in partial fulfilment of the
requirements for the degree of
Master of Mechanical Engineering

Department of Energy Sciences
Division of Fluid Mechanics
Lund University

February 2011

Abstract

Large eddy simulations of full geometry wind turbines, employing the virtual boundary method, have been carried out with the in-house developed CFD-code at the Division of Fluid Mechanics. The aim is to study the influence of pitch variation on the wake interaction between two wind turbines, and investigate some of the characteristics related to the performance and reliability of the CFD-code.
Successful full geometry simulations can avoid the faults introduced by assumptions made in modelling the blades, thus introducing increased possibilities of investigating the physical characteristics of wind turbine wakes. Characteristics which are important in the design process of wind turbines and in the design of wind farms.
The simulations proved to be able to capture the influence of pitch control. Initial indications of wake meandering have also been shown. There, are however; issues compromising the results, implying a need of further development within the treatment of the boundaries of the blades and increased dimensions of the spatial domain.

Sammanfattning

Strömningssimuleringar av vindkraftverks fulla geometri har genomförts med LES och virtual boundary-metoden. CFD-koden som använts för beräkningarna är utvecklad av forskare på avdelningen för Strömningsteknik vid Lunds Universitet. Målet med simuleringarna har varit att studera hur variation av pitch-vinkeln påverkar interaktionen mellan två vindkraftverk, och därigenom även kunna undersöka hur väl CFD-koden presterar.

Framgångsrika simuleringar av vindkraftverks fulla geometri kan ge mer tillförlitliga resultat än de som fås då rotorn representeras av förenklade modeller. Detta introducerar nya möjligheter att studera och bestämma vindkraftsvakars egenskaper. Egenskaper som är viktiga vid design av vindkraftverk och vid utformningen av vindkraftsparker.

Simuleringarna som utförts visar att det är möjligt att fånga påverkan av variation av pitch-vinkeln. Indikationer finns även på att så kallad wake meandering är möjlig att påvisa i simuleringarna. Det finns dock svagheter som komprometterar resultaten, och visar att det finns behov av vidareutveckling av hur bladens gränsskikt behandlas och behov av större dimensioner av domänen.

Acknowledgements

This degree project has been carried out at the Division of Fluid Mechanics, Lund University, and supervised by research assistant Robert-Zoltán Szász. I wish to express my sincere appreciation to Robert for his enthusiastic support and excellent supervision within both CFD and computer science.
Particular thanks to student colleague Jonas Krüger for the fruitful cooperation in developing post-processing tools, and for many interesting discussions.
Thanks to the Center for Scientific and Technical computing LUNARC, for providing the computational resources for this degree project.
A special thanks to Jan-Åke Dahlberg at Vattenfall Vindkraft AB for a very rewarding introduction to the field of wind turbine aerodynamics and the needs within the industry.
I would also like to thank the all staff at the Division of Fluid Mechanics and the Division of Combustion Physics, for making me feel welcome.
Special thanks to Michaël Edon for allowing me to use the wind turbine geometry of your internship project.
Finally I would like to thank all of the researchers who have contributed to development of the in-house CFD-code, which has been essential for this degree project.

Lund, February 2011

Sten Edström Barup

Nomenclature

Roman letters

A	disc area	$[m^2]$
A_p	planform area	$[m^2]$
A_r	swept rotor area	$[m^2]$
C	CFL number	[-]
C_d	drag coefficient	[-]
C_l	lift coefficient	[-]
C_p	power coefficient	[-]
$\mathbf{D}$	drag force	$[N]$
d	disc diameter	$[-]$
E	turbulent kinetic energy	[J]
f	frequency of wake meandering oscillations	$[Hz]$
k	wavenumber	$[Hz]$
L	characteristic length	$[m]$
$\mathbf{L}$	lift force	$[N]$
p	pressure	$[Pa]$
P	kinetic power	$[W]$
P_m	mechanical power	$[W]$
u, v, w	velocity components in x, y, z direction respectiely*	$[m]$
U	characteristic velocity	$[m/s]$
U_∞	undisturbed wind speed	$[m/s]$
U_{rel}	relative wind speed	$[m/s]$
U_{ref}	reference speed	$[m/s]$
w_{hub}	velocity component in z direction at hub height	$[m]$
Re	Reynolds number	[-]
R	rotor radius	[m]
St	Strouhal number	[-]
t	time	$[s]$
Δt	time step	$[s]$
Δx	distance between nodes	$[m]$
x, y, z	spacial coordinates*	$[m]$
x_hub	vertical hub position	$[m]$

Greek letters

α	angle of attack	[°]
β	Hellmann's constant	[-]
Ω	angular velocity	[rad/s]
λ	tip speed ratio	[-]
θ	pitch angle	[°]
ρ	density	$[kg/m^3]$
ν	kinematic viscosity	$[m^2/s]$

Acronyms

BE	Blade Element
BEM	Blade Element Momentum
CFD	Computaitonal Fluid Dynamics
CFL	Courant-Friedrichs-Lewy
DFT	Discrete Fourier Transform
DNS	Direct Numerical Simulations
EWEA	European Wind Energy Association
HAWT	Horizontal Axis Wind Turbine
LES	Large Eddy Simulations
LTH	Lunds Tekniska Högskola
MEXICO	Model rotor EXperiments under COntrolled conditions
NREL	National Renewable Energy Laboratory
NS	Navier-Stokes
PIV	Particle Image Velocimetry
RANS	Reynolds Averaged Navier-Stokes
RMS	Root Mean Square
TSR	Tip Speed Ratio
VAWT	Vertical Axis Wind Turbine
WRD	Wind Rotor Design system
WT	Wind Turbine

*Normalized values of the parameters can be found in chapter 5 due to the implementation of the CFD-code.

Contents

List of Tables

List of Figures

Chapter 1

Introduction

This chapter will give an introduction to wind power and wind turbines. It begins with a review of the history of wind power, followed by descriptions of the characteristics of wind turbines and wake structures. The last section briefly summarizes the industry trends and development needs.

1.1 History

The extraction of power from the wind is not a new phenomenon as will be described within this section. A review of the history of wind power will be presented, based upon the book *Wind Turbines Fundamentals, Technologies, Application, Economics* [26] by Hau and von Renouard, to which the interested reader is referred to for further deepening.

There are authors claiming that there are evidences that prove human usage of wind for generating mechanical power as far back as 3000 years ago. However, there are reliable evidences from year 644 B.C. describing the existence of windmills in the region of Seistan on the Persian-Afghan border. These were used for milling grain and there has been found a sketch of a vertical windmill from year 945. Early use of vertical windmills has also been the case in China, but here for draining rice fields.

Reliable information about the existence of horizontal windmills in Europe originates from year 1180, in the region of Duchy of Normandy. The windmills were mainly used for milling grain and spread rapidly across the whole of Europe. About 200 000 windmills are estimated to have existed in Europe in the middle of the 19th century, later gradually decreasing because of the introduction of steam engines.

This was also the century when windmill technology reached the USA. The development was driven by the lack of natural surface water in the plains of the Mid-West. Therefore, a method for pumping water from wells was needed. This need proved to be possible to satisfy by wind wheel pumps in the early 19th century. Major improvements of the wind wheel pumps were made by the mechanics Daniel Halladay in the mid 19th century. He managed to develop a self regulating wind-wheel that among other things controlled the power through pitching the blades. By 1930 there were about 100 factories and there had been more than six million wind wheel pumps manufactured in the USA. The number gradually decreased as the "Rural Electrification Program" was initialized in 1930.

The electrification progress of the rural areas were, due to the large distances, much slower in the USA than Europe. This is probably the reason why some of the early attempts of generating electricity from the wind were made by converting wind wheel pumps. However, more successful undertakings were made in Denmark by professor Poul La Cour with the same objective, electrifying the rural areas. Encouraged by the government he built his first electricity producing wind turbine in 1891.

The development during the first and second World War were mainly encouraged by high fossil fuel prices. Undertakings were not only made in Denmark, but also in other countries within Europe, especially Germany. The focus in Germany was rather on large scale electricity production than electrifying rural areas. Many ambitious plans were made, but only a few were realized, often with poor results due to lack of financing among other things.

The fuel crisis of the seventies renewed the interest of alternative electricity generation and large scale development projects were assessed and financed by governments in e.g. Germany, USA and Sweden. Large wind turbine prototypes in multi MW sizes were built. However few of these projects turned out as successful as hoped, in many cases probably because of lack of previous experiences and starting with too large turbines. Most successful were the smaller Danish wind turbines, often manufactured at factories, usually producing agricultural equipment. The customers were usually farmers, for which the investments were favorable due to governmental subsidies. During the late seventies subsidies were also introduced in the State of California resulting in a gold rush mentality within the private sector of so called "wind farmers". About 40 % of the wind turbines erected in California by 1987 were delivered by manufacturers in Denmark, contributing to the development of which we can see the results today.

1.2 Characteristics of wind turbines

The horizontal-axis three-bladed upwind wind turbine is the predominate design today. Nevertheless a great variety of devices to convert the energy from the wind has been developed, and there is still development in progress. There is, however; yet no device able to compete with the *horizontal-axis wind turbine* (HAWT). The two most common disadvantages of other designs, such as the *vertical-axis wind turbines* (VAWT), is firstly the difficulties to regulate the power generated in high wind speeds, and most importantly the low efficiency. One of the reasons of the success of the HAWT can be addressed to the benefits of the preceding knowledge within propeller and airfoil design. A HAWT has been simulated within this degree project and will therefore be the one to be further described. Figure 1.1 illustrates a HAWT, which consists of four geometrical main components: rotor, nacelle, tower and foundation. The blades are attached to a hub, which together form the rotor. [26]

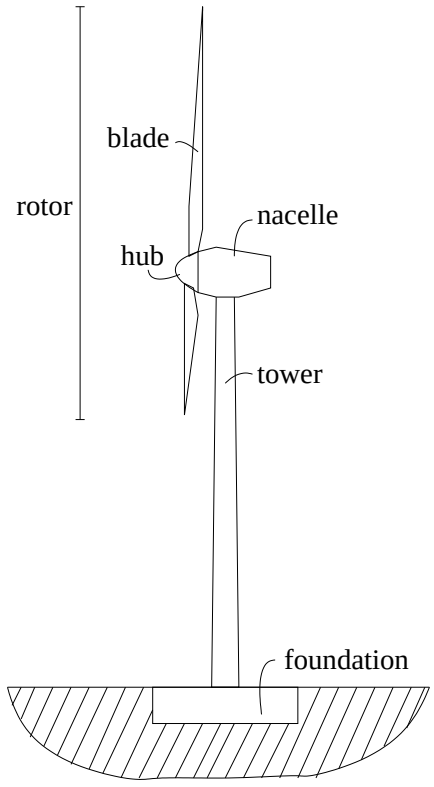

Figure 1.1: Components of a HAWT

The following subsections will give an introduction to the characteristics of the rotor. The first will describe the basic features of a rotor design, and is followed by two brief descriptions of common rotor models. The last subsection goes further into power control.

1.2.1 Rotor design and characteristics

The *power coefficient* is a measure of how efficient a wind turbine rotor is at extracting power from the wind, formulated as:

$$C_p = \frac{P_m}{\frac{1}{2}A_r \rho U_\infty^3} \tag{1.1}$$

where P_m is the mechanical power-output from the rotor, A_r the swept area of the rotor, ρ the density and U_∞ the free stream flow speed. The coefficient is thus the mechanical power to available-wind-power quota. It has a theoretical maximum due to mass conservation of 0.593 according to Betz limit, formulated by the German aerodynamicist Albert Betz in 1926. The actual limit is however lower since the actuator disc method has been used in the derivations, with assumptions which are not necessarily valid (e.g. no flow rotation). The actuator disc method will be further described in section 1.2.3. [26]
Modern wind turbine blades are designed from one or multiple airfoils and relies on their aerodynamic lift properties for power generation, resulting in power coefficients of modern state-of-the-art wind turbines of almost 0.5. The traditional windmill relies on aerodynamic drag, which results in a maximum theoretical power coefficient of 0.2. [26]
The characteristics of an airfoil is usually described by it's *drag* and *lift coefficients*, C_d and C_l respectively, which are available through experimental results for a large variety of airfoils. These coefficients are normalized forces acting in parallel and perpendicular direction with the direction of the oncoming flow, as can be seen in figure 1.2, where U_{rel} is the relative wind speed approaching the airfoil, α the *angle of attack*, θ the *pitch angle*, **L** denotes the *lift force* and **D** the *drag force*.

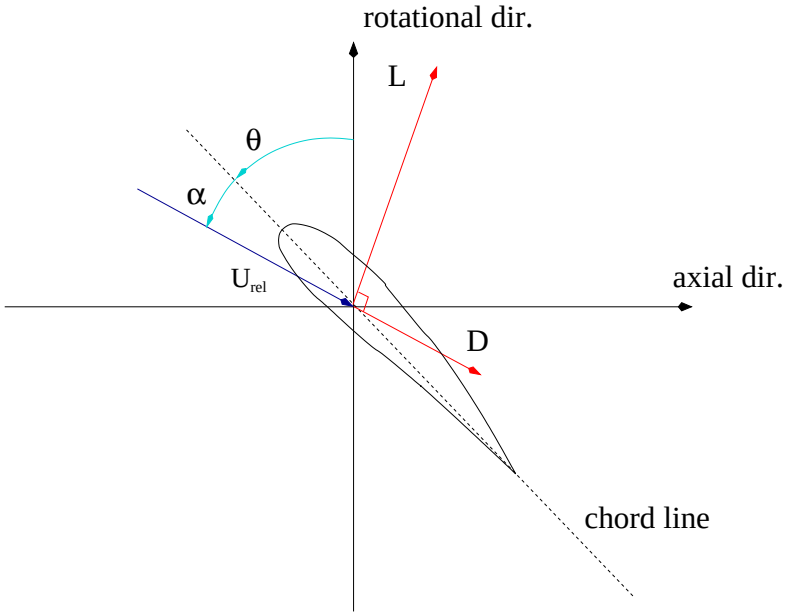

Figure 1.2: Airfoil with drag and lift forces, relative velocity and angles defined

The drag and lift coefficients are dependent upon the *Reynolds number* (Re) (defined in section 3.3) and the angle of attack, and are given by the following equations:

$$C_d(Re, \alpha) = \frac{\mathbf{D}}{\frac{1}{2}U_{rel}^2 A_p \rho} \tag{1.2}$$

$$C_l(Re, \alpha) = \frac{\mathbf{L}}{\frac{1}{2}U_{rel}^2 A_p \rho} \tag{1.3}$$

where A_p is the plan-form area given from the product of the *chord length* and *span width* of the blade. [26]
It is desirable to maximize the drag-to-lift ratio in order to achieve high torque and thereby high power. This is not only achieved by choosing the best airfoil, but also twisting and tapering the blade. The twist is made around the span-wise axis to optimize the angle of attack as the relative wind direction varies along the radius. The tapering is achieved by gradually decreasing the chord length toward the tip of the blade, and is partly made to optimize blade performance, but also for structural and economic reasons. Since the lift and drag coefficients of an airfoil are strongly dependent on the relative wind speed, through the Reynolds number, it is desirable

to vary the airfoil geometry along the span-wise direction. For this purpose there has been developed airfoil families, typically consisting of about three airfoil geometries optimized for different Reynolds numbers. [9]
The speed of rotation of the rotor is an important characteristic of a wind turbine rotor and in the design process of a wind turbine blade. It is often described by the *tip-speed ratio* (TSR) which is a normalized value of the speed of rotation formulated as:

$$\lambda = \frac{\Omega R}{U_\infty} \tag{1.4}$$

where Ω is the angular velocity, R the rotor diameter and U_∞ the undisturbed wind speed. The theoretical optimum tip-speed ratio of a three bladed rotor is according to Wizelius [28] around 7. [28]

1.2.2 Actuator disc method and momentum theory

In the *actuator disc method* one simplifies the rotor into a thin actuator disc characterized by a pressure drop in the flow direction. The pressure change is caused by the momentum loss due to energy extraction through the disc, illustrated in figure 1.3. The stream tube shown in the figure is an imaginary surface representing the limits of a constant mass flow, thus increasing the cross-section as the axial velocity is decreasing. The following assumptions are made in the actuator disc method:

- incompressible flow
- uniform and steady flow upstream
- steady and uniform velocity at the disc
- the mass-flow upstream and downstream is contained within the stream-tube
- no flow rotation produced by the disc

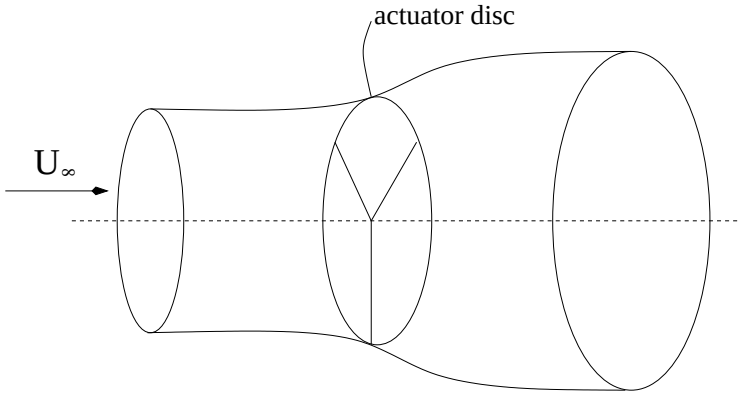

Figure 1.3: Actuator disc and stream tube.

The method was employed by Albert Betz to derive the afore mentioned Betz limit. [9]
There are means of taking wake rotation into account in the momentum theory by introducing multiple stream tubes along the radius. The change in rotation through the actuator disc is determined for each stream tube. This makes it possible to consider the kinetic energy generated in the wake due to the torque extracted by the rotor. Increased torque results in higher kinetic energy in the wake and thereby higher energy losses, which makes it preferable to operate at higher rotational speeds rather than higher torque for the same power. This connection is described by Glauerts optimum which differs from Betz limit by it's dependence upon rotational speed. Glauerts optimum touch upon the Betz limit asymptotically as the rotational speed increases. [12]

1.2.3 Blade element momentum method

The *blade element momentum* (BEM) method is often used to evaluate and develop blades for wind turbines. This method is derived from a combination of momentum theory with wake rotation and the *blade element* (BE) model. The latter can briefly be described by dividing a wind turbine blade into multiple sections along the span direction, and through knowing the oncoming velocity, angle of attack, lift and drag coefficients for each section, calculate the contributing torque and thrust force. By adding together the contributions from all sections and multiplying with the number of blades one gets the total torque and thrust of the rotor. The thrust force is the force acting in axial direction, causing a bending torque on the blade and tower. Fol-

lowing assumptions are made in the BE model: [12]

- flow interaction between blades negligible
- flow along the length of the blade negligible
- representative values for lift and drag characteristics available for each blade section
- oncoming flow parallel with axis of rotation (possible to consider variations in flow direction by extended model)
- a sufficient number of sections used

It is possible to include semi-empirical models for the contribution of drag forces due to tip and root vortices, to the blade element model. [26]
The BEM method is derived by setting the torque and thrust equal between the BE model and the momentum theory with wake rotation. This simple combination implies that the influence of the assumption of finite number of blades made in momentum theory is negligible. If this is not valid one can make use of different tip correction functions, of which Prandtl's tip correction function often is preferred. BEM in the basic formulation is neither valid for heavily loaded turbines for which the axial flow induction will be too large. However empirical correction methods are available. [9]
An often applied practice is to neglect the drag coefficient since, in pre-stall operation, it is much smaller than the lift coefficient for wind turbine airfoils [12]. It is however not unusual that wind turbines occasionally operate in post-stall conditions, for which the drag coefficient increases significantly and thus cannot be neglected. [9].

1.2.4 Power control

Power control is necessary since wind turbine generators generally reach their rated power at wind speeds much lower than the maximum wind speeds available. The generator would be overloaded at high wind speeds without power control, causing breakdown. The structural design would also suffer severe damage from too high torque and thrust, and too high rotational speeds. There are two aerodynamic main

methods for power control, which in turn can be achieved by different technical methods. The aerodynamic methods relies on either stall or pitch control.
Stall occurs when the flow detaches from the low-pressure side of an airfoil which significantly decreases the lift force. Control by stall can be either active or passive, which is determined by whether any mechanical equipment is used to vary the properties of the wing or not. The detached flow can be a result of high angle of attack or modifications in blade geometry by e.g. moving spoilers. Moving spoilers are categorized as an active stall mechanism as-well as mechanisms rotating the blade to increase the angle of attack. The angle of attack will also increase if the wind speed increases without any significant change in rotational speed, which is called passive stall.
The mechanism for pitch control resembles the mechanism for active stall through blade rotation. The difference is the direction of rotation, which for pitch control decreases, the angle of attack towards feathered position to decrease the torque. Pitch control require larger angular adjustments than the equivalent active stall control. Pitching the blade towards feather reduces the thrust-force on the rotor and tower which is advantageous in high wind speeds since the structural stresses decreases. This effect is not achieved with stall regulation which makes it necessary to design stall regulated wind turbines to higher structural load conditions. This is one of the reasons for the dominance of pitch controlled turbines among large wind turbines.
Stall control, and especially passive stall control, require less complicated mechanisms and have therefore traditionally been used for small wind turbines to ensure reliability and low production and maintenance costs. Passive stall control is, according to Hau and von Renouard [26], often referred to as the "Danish Line" since Danish manufacturers have used and refined this method. Pitch control is however also extensively used by Danish manufacturers. Fast and precise regulation can be achieved more easily with pitch control than stall control which is desirable to ensure highest possible power-output and decrease fluctuations in generator loading.
The need of precise control is dependent on which kind of transmission and generator is used. There are two main designs and their combinations. The classic design has a gearbox connecting the rotor with a conventional, four pole, generator. The second design has no gearbox and relies instead on a less traditional generator with many poles and an inverter which increases the electric current frequency to make it compatible with the grid frequency. [26]

1.3 Wake structures

The physics of wind turbine wake structures in different conditions are not yet fully understood, and is a topic of progressive research. There are, however; some established characteristics, mainly concluded from experiments, which will be described within this section. The wake is a result of the energy extraction from the wind, which decelerates the flow behind the turbine, thus reducing the kinetic energy. The kinetic energy in the wind is also partially transferred into turbulence by the rotor. Further more the extraction of torque by the rotor results in a counter-wise rotation of the wake due to the preservation of momentum. Flow structures called tip and root vortices are considered to be important characteristics of the wake and will be described below, followed by a brief review on wake meandering.

1.3.1 Vortex structures

Vortex structures trailing from the tips and roots of the blades, has been concluded from experiments by e.g. Alfredsson and Dahlberg in [8]. These structures is a well established characteristic of finite airfoils, also prevalent at e.g. the wingtips of airplane wings. A simple way of explaining the creation of the tip and root vortices is that they are produced due to the pressure difference over the wing or blade, which results in a flow towards the low pressure side at the ends of the wing span. The vortices are also affected by the surrounding flow, thus transported down streams with it. The trailing vortices behind a wing gradually break down due to dissipation by viscosity as they travel down stream. The interested reader is referred to White [27] for deepening within airfoil theory.

In reality multiple trailing vortex structures are generated along a wing or blade, merging some distance behind the tip and root regions. [27] The rotation of a blade on a wind turbine complicates the analysis and path of the trailing vortex structures compared with an equivalent airplane wing. The path of the vortices is illustrated in figure 1.4. Another effect is that the vortices at the root region unite further downstream than the ones at the tip region. The surrounding flow is also expected to influence the path, with it's variations in flow speed along the radial direction, partly caused by the obstruction by the hub. The down stream travel distance between two adjacent tip vortices is referred to as the wake pitch, and is dependent on both rotational velocity and axial flow velocity.

Further more trailing vortex structures from different blades pair up behind the rotor,

contributing to the break down of the structures. The break down, and the distance from the rotor at which it occurs, is not only dependent on the wake pitch and pairing, but also the ambient turbulence. Higher ambient turbulence will give a less stable wake, earlier break down and thus also a shorter wake. The ambient turbulence is lower at offshore sites, resulting in a long wake behind the first turbine in a row. The turbulence generated in the first wake will result in a shorter wake behind the second turbine. This effect will be similar for wind turbines further down stream, thus indicating that the second wind turbine in a row will be the most exposed to fatigue loads. [12]

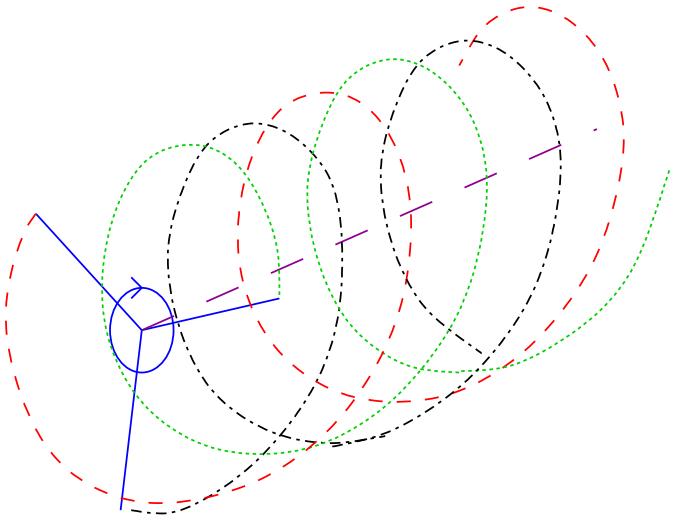

Figure 1.4: Tip-vortex paths trailing the blades shown by the curved lines, path of three root vortex cores shown by the dashed line through the rotor center.

1.3.2 Wake meandering

Large scale vortex shedding is a well known characteristic of bluff body wakes. The large eddies, produced in the vicinity of the body, are determined by the shape and size of the body. This information is consequently transported downstream, in some preconditions resulting in large scale oscillations called *wake meandering*. Wake meandering is connected to the dimensionless *Strouhal number* (St):

$$St = \frac{fL}{U_\infty} \tag{1.5}$$

where f is the frequency of the wake meandering oscillations, L is the characteristic length of the body and U_∞ is the undisturbed wind speed. The Strouhal number of wake meandering valid for a circular disc is around 0.12, which according to Medici [14] is close to what should be expected for wind turbines operating at high tip-speed ratios. Furthermore the Strouhal number should increase if the tip-speed ratio decreases. The characteristic length is the rotor or disc diameter. [14]

1.4 Industry trends

The wind power industry is a growing market and one of the components in the ambitions of a more sustainable electric power system. The scenario for wind energy production in Europe is according to the *European Wind Energy Association* (EWEA) an increase from 137 TWh in 2008 to 582 TWh in 2020. Hence in 2020 the wind energy share would be 16.9 % of the total electricity production in Europe and the annual investments €23.5 billion, of which €8.8 billion in offshore wind power capacity. [29]

These large numbers in both production and investments implies that even a small gain in production by optimization results in large benefits. Barthelmie et al. states in [4] that the standard methods used within the industry for wake modelling is inadequate, and over-estimates the power production, for offshore wind farms. Furthermore the same authors conclude that there is a "*gap between engineering solutions and CFD models, and a bridge is needed between these in order to provide more detailed information for modelling power losses, for better wind farm and turbine design and for more sophisticated control strategies and load calculations*" [4].

Most of the commercial software used today for wind farm power estimations originates in models developed in the 1980s. These models are providing accurate estimations of power production in small wind farms and simple terrain, but are less accurate in other conditions. [4]

Since the large scale expansion in wind power is expected to take place in large wind farms at offshore and mountainous sites, it is of great importance to be able to predict the outcome of these projects.

Chapter 2

Background

This chapter will give a overview of the background of this degree project, describing the aim and objectives and project resources. The reader will also be introduced to some of the related work carried out within the topic.

2.1 Aim and objectives

The progressive development of computer performance and the decreasing costs have paved the way for the high performance computing needed to make *computational fluid dynamics* (CFD) useful for complex simulations. As it will be shown in section 2.3, great achievements have been made during the last fifteen years within the topic of CFD simulations on wind turbine wakes. Most of these achievements are based on modelling the influence of the geometries rather than including the real geometries of wind turbines into the computations. Such measures are taken due to the physical complexity of, and computational efforts needed to, evaluate the flow field and boundary layers surrounding the rotor. However, successful full geometry computations can make it possible to avoid the faults introduced by assumptions, made in attempts of modelling. It will then result in increased possibilities to investigate the physical characteristics of the flow, of which many properties are not fully understood today. This is not only of interest for development and optimization of new blade-geometries, but also of great importance when designing wind farms and investigating the aerodynamic influence of landscapes and obstacles.
The aim of this degree project is to make a contribution to the knowledge in CFD simulations of full geometry wind turbines. The objectives are:

- Implementation of a realistic wind turbine geometry.
- Stipulate a suitable set of cases with a real application.
- Perform and analyze large eddy simulations of the cases.
- Evaluate some characteristics of the performance and reliability of the CFD-code from the results of the simulations.

The first objective is to implement a realistic wind turbine geometry. The second objective involves an investigation of which cases are suitable to investigate within the scope of this degree project. The third, and main objective, involves the computational effort and the following analysis. This is followed by an evaluation of the performance of the CFD-code, and a discussion on the reliability.
The choice of cases to investigate has been made from two perspectives. The first is that the cases should have a connection with a topic of interest to investigate for real applications. The second is that it should be possible to evaluate some of the characteristics dealing with the reliability and performance of the CFD-code from the results of the simulations.
From the above mentioned requirements a decision was made to investigate the influence of changes in angle of attack, which is made by pitching the blades. The cases consists of two wind turbines in a row by their full geometries. Two cases are set-up with different blade-pitch settings for the first wind turbine, further described in section 4.3.
The real application for pitch control is mainly power control, which is necessary to reduce the power at high wind speeds, but can also be of interest for purposes such as sound emission limitations, structural load limitations and wind farm optimization. The latter one is an application with development in progress at e.g. the Swedish offshore wind farm Lillgrund, according to Jan-Åke Dahlberg at Vattenfall [7]. It is thus of interest to investigate to what extent it is possible to optimize the total power-output and decrease the structural loads by pitch-control. The variation in pitch is also a measure to investigate the sensitivity of the CFD-code to geometric changes. The changes in geometry due to pitch change should affect the computed wake-structure and estimated power-output.
This degree project is a contribution to research in progress at the Division of Fluid

Mechanics where the CFD-code used for the computations has been developed. More about the software is to be read in section 2.2.

2.2 Project resources

The resources that have been used within this degree project will be described within this section. These resources can be divided into three categories: software, computational and human resources.
The software used for the computations is an in-house CFD-code written in Fortran, developed by several researchers at the Division of Fluid Mechanics. The code can be described as a laboratory for the CFD researchers at the division, where different methods and approaches can be implemented and evaluated. Two examples of previous research carried out with the code is [16] by Ohlsson and Fuchs and [17] by Revstedt. The version used within this study has previously been used in e.g. [23] by Szász, and no changes have been made to the code during this degree project. Post-processing has been carried out with both previously existing in-house Fortran programs and Fortran programs developed by the author in cooperation with Jonas Krüger. Grace [1] and OpenDX Data Explorer [2] has been used for visualizations.
The computational resources for the CFD computations have been delivered by the center for scientific and technical computing LUNARC at Lund University. The computer cluster Platon with 216 nodes has been provided. The cores used for the simulations are arranged in 8 cores per node and have a clock rate of 2.26 GHz. 2,900 megabytes of memory have been allocated for each core during the simulations. Post-processing has been carried out at a standard laptop.
Research assistant Robert-Zoltán Szász has supervised this degree project, and thus been an essential resource. Cooperative efforts have been made by the author and Jonas Krüger, mainly on post-processing software but also with discussions along the way. Jonas Krüger has carried out a diploma project in an adjacent topic within wind turbine simulations. Jan-Åke Dahlberg at Vattenfall Vindkraft AB contributed with and introduction on the relevant topics from the industry's point of view and a summary of how the research has developed from the seventies until today [7]. Further more have the PhD students at the division been providing many different kinds of help and input.

2.3 Related work

Studies made on wind turbine wakes can be divided into simulations and experiments. The amount of research within the topic is substantial and the progress is continuous. Another well established subdivision within the topic is the distinction made between *near-wake* and *far-wake* studies. The near-wake studies focus on the flow in the immediate vicinity of the rotor, much characterized by the flow around the blades. In far-wake studies the main objective is to investigate interaction phenomenas e.g. between wind turbines in wind farms. Since the work performed within this master thesis project aims at investigating the far-wake, this is what will be focused upon. The formation of the far-wake is however the result of the near-wake, which thus cannot be neglected. The first two subsections are brief summaries of the achievements made in experiments and simulations. The third section is a short summary of the rotor design characteristics, provided by Edon in [10] from which the rotor design used within the simulations originate.

2.3.1 Experiments

Early work within experimental wake studies in wind tunnels was performed by e.g. Alfredsson and Dahlberg [8] in the late seventies. The evaluation methods used were hot-wire anemometry for quantitative results and smoke visualizations. More recent experimental studies by Medici in e.g. [14] have provided evidence of the wake meandering phenomenon described in section 1.3. Even more recent work has been performed within e.g. the *MEXICO* (Model rotor EXperiments under COntrolled conditions) [19] where pressure sensors and *Particle Image Velocimetry* (PIV) has been employed to evaluate the flow structures. The PIV-images sampled do not only provide increased knowledge on the flow structures, but are also important data for evaluation and validation of CFD codes and methods. Such evaluation work is essential to ensure consistency of the results and ensure the reliability of the simulations. Wind tunnel measurements are often preferable to field experiments for validations, since the conditions are well known. This ensures correlation between the set-up of experimental and computational cases. The drawback of wind tunnel studies are however that in most cases, only the near-wake characteristics are possible to investigate because of the limited space. The limited space also makes it impossible to use full-scale wind turbines, thus introducing scaling issues. The American *NREL* (National

Renewable Energy Laboratory) experiments at NASA Ames [18] performed in 1999 are also worth to be mentioned as a large experimental work carried out recently.

2.3.2 Wake simulations

BEM, described in section 1.2.3 is the predominant method used to predict performance of wind turbines within the industry. Since the method relies on empirical data, and engineering models for dynamic events, it does not always manage to deliver accurate predictions. This can according to Ivanell [12] be explained by the 3-D effects not taken into account for in BEM and insufficient empirical input.
CFD simulations on wind turbines are expected to be able to provide more accurate predictions for the 3-D flow characteristics. The CFD methods have gradually evolved during the nineties and received an impetus in the new century.
Two of the early numerical studies of far-wakes were presented by Ainslie [3] in 1988 and by Crespo and Hernndez [6] in 1996. Both studies developed numerical models of the far-wake of wind turbines from the *Navier-Stokes* (NS) equations (NS equations further described in section 3.1). According to J.N. Sørensen [20] the first near-wake full Navier-Stokes simulations for a complete rotor was presented by N.N. Sørensen in 1998, using RANS. Today approaches relying on either RANS or LES (further described in section 3.3) are prevalent within the research field of far-wakes. Different paths for introducing the effects caused by the rotor on the flow field have evolved to enable far-wake studies. The need of introducing rotor models is due to the difficulties with resolving the wide range of scales in the flow, ranging from boundary layer turbulence to large-scale motions in the size of the rotor diameter. One example is the actuator disc model which represents the rotor by introducing surface forces to the flow field, corresponding to the mechanical work extracted by the rotor. The strength of the surface forces is given by modified experimental 2-D data of lift and drag forces, smeared over the surface of the actuator disc. Early results achieved by this model in wind turbine simulations were presented by J.N. Sørensen and Myken [21] in 1992. The model has more recently been employed by Ivanell [12] in 2009, where simulations with the actuator line model also have been carried out. The surface forces in the actuator line model are introduced along lines representing the blades where the magnitude is constantly evaluated from the local angle of attack and tabulated airfoil data. The actuator line model employed by Ivanell was introduced by J.N. Sørensen and Shen in [22]. Successful simulations of a wind farm containing 80 wind turbines, capturing the main production variations, was carried out by Ivanell, using

the actuator disc model.
Another wind turbine rotor model is the vorticity transport model recently used by Fletcher and Brown [11] and previously used for studies on helicopter rotors. This model is carried out by evaluating the vorticity-velocity formulation of the NS equations. The rotor is modelled through the bound vorticity distribution evaluated by an extension of the lifting line theory. The cases investigated by Fletcher are involving simplified interactions between two rotors.

2.3.3 Rotor design characteristics

The rotor design implemented in the simulations of this master thesis has been developed by Edon [10]. The geometry of the rotor is described in section 4.1.1, whereas this section focuses on the operational characteristics of the rotor, as this relates to what should be expected from the results. Table 2.1 shows the predicted mechanical power extracted from the wind with and without pitch control. The figures are given for both cases since this increases the understanding for the dynamics of the rotor, which might give indications on the accuracy of the results obtained from the simulations. The data presented in table 2.1 are predictions evaluated by the BEM method in the software *Wind Rotor Design System* (WRD). This software has been developed by Nordic Folkecenter for Renewable Energy in Ydby, Denmark. The predictions are according to Edon [10] comparable to data for commercial blades, but should according to a clarification by email (Sept 10) be considered as a first approach study where only laminar flow is considered. The simulations carried out within this degree project include turbulence and 3-D effects, thus expectable to more accurately reflect the physics of the actual flow. Large Eddy Simulations also introduce the possibilities of investigating the flow-field into detail and interaction between turbines, which this degree project will contribute with.

Table 2.1: Operational characteristics and performance for rotor, reproduced tabular after [10]

OP-char.	no regulation			pitch regulation			
wind speed	rpm	power	C_p	pitch	rpm	power	C_p
2	5.3	11.5	0.486	0	5.3	11.51	0.486
4	9.0	96.60	0.510	0	9.0	96.60	0.510
6	13.5	326.0	0.510	0	13.5	326.0	0.510
8	18.0	772.8	0.510	0	18.0	772.8	0.510
9	20.3	1100	0.510	0	20.3	1100	0.510
10	22.5	1509	0.510	0	22.5	1509	0.510
11	24.7	1983	0.510	2.0	22.5	1817	0.461
12	27.0	2502	0.510	5.0	22.5	1826	0.357
14	31.5	3645	0.510	8.8	22.5	1822	0.224
16	36.0	4434	0.510	11.7	22.5	1817	0.150
18				14.6	22.5	1834	0.106
20	45.0	12074	0.510	17.5	22.5	1814	0.077

Chapter 3

Numerical Methods

The modelling of the governing equations and turbulence, and the numerical theory will be briefly described within this chapter. The aim is to give an introduction to CFD and state the numerical methods used for the computations. No detailed descriptions will be made of the methods since no new methods have been implemented or developed as a result of this project.

3.1 Governing equations of fluid dynamics

CFD is based on evaluation of the governing equations of fluid dynamics, also refereed to as the Navier-Stokes equations. It is a mathematical model of the dynamic behavior of fluids and consists of the following equations:

- continuity equation
- momentum equations
- energy equation

Incompressibility has been assumed in the simulations since the mach-numbers in the flows are low. The equations presented bellow are all formulated with this assumption.
The fulfillment of the continuity equation ensure that mass is conserved for the fluid. The equation is, in a three dimensional cartesian coordinate system, formulated as:

$$\frac{\partial u}{\partial x} + \frac{\partial v}{\partial y} + \frac{\partial w}{\partial z} = 0 \tag{3.1}$$

where u, v, and w are the velocity components in x, y and z direction respectively. The momentum equation is derived from *Newton's second law of motion* and describes that the rate of change of momentum is equal to the sum of forces acting on the fluid. Making assumptions of constant density and kinematic viscosity (ν) gives the following formulation:

$$\frac{\partial u}{\partial t} + u\frac{\partial u}{\partial x} + v\frac{\partial u}{\partial y} + w\frac{\partial u}{\partial z} = -\frac{1}{\rho}\frac{\partial p}{\partial x} + \nu\frac{\partial^2 u}{\partial x^2} + \nu\frac{\partial^2 u}{\partial y^2} + \nu\frac{\partial^2 u}{\partial z^2} \tag{3.2}$$

$$\frac{\partial v}{\partial t} + u\frac{\partial v}{\partial x} + v\frac{\partial v}{\partial y} + w\frac{\partial v}{\partial z} = -\frac{1}{\rho}\frac{\partial p}{\partial y} + \nu\frac{\partial^2 v}{\partial x^2} + \nu\frac{\partial^2 v}{\partial y^2} + \nu\frac{\partial^2 v}{\partial z^2} \tag{3.3}$$

$$\frac{\partial w}{\partial t} + u\frac{\partial w}{\partial x} + v\frac{\partial w}{\partial y} + w\frac{\partial w}{\partial z} = -\frac{1}{\rho}\frac{\partial p}{\partial z} + \nu\frac{\partial^2 w}{\partial x^2} + \nu\frac{\partial^2 w}{\partial y^2} + \nu\frac{\partial^2 w}{\partial z^2} \tag{3.4}$$

where p is the pressure,t time, and ρ density. Body forces have been excluded from the equations since the major prevalent body force, namely the gravity force, can be neglected since no buoyancy effects are expected. The local acceleration is described by the first term from the left. The following three terms are referred to as the convective terms. On the right-hand side the first term denotes the pressure gradient and the terms of second order derivatives in space are the diffusion terms. The energy equation ensures the energy conservation of the flow and is derived from the *first law of thermodynamics*. This equation is however not evaluated during the computations since the cases are assumed to be isothermal.

3.2 Discretization

The governing equations are a system of non-linear differential equations, which can not be analytically evaluated for most engineering flows. Numerical methods are therefore used to solve the flow field in a discrete manner. This is generally referred as *Computational Fluid Dynamics* (CFD). The numerical approach requires discrete descriptions of:

- space
- time
- the governing equations

The discretization in space is performed by generating a *grid*, also called *mesh*, within the volume of the flow field to be evaluated. Time-steps are introduced in unsteady computations to handle continuous fluctuations in the flow in a discrete manner.

There are three common methods available for discretization of the governing equations, *finite volume*, *finite difference* and *finite element* method. The one provided with the in-house CFD-code is the finite difference method which has the advantages of simple implementation on cartesian grids, and enabling the use of accurate high order schemes. Unlike the finite volume method it does however not ensure mass conservation unless special care is taken. The interested reader is referred to e.g. [25] for the formulation of the different discretization methods.

The finite difference method more or less require a structured cartesian grid, which is the case for the CFD-code used. The grid is staggered and it is possible to make local refinements. The main drawback with a cartesian grid compared with a unstructured grid, is the difficulties associated with irregular and curved boundaries to which the cartesian grids are difficult to adapt and refine. The in-house CFD-code treat this by the virtual boundary method further described in section 3.4. Cartesian staggered grids do however require less computational resources compared to unstructured grids. They are also suitable for cases that require high resolution in all directions according to e.g. Lörstad [13], which is the case for LES (further described in section 3.3).

The performance of the solver is increased by the use of multi-grid in four global levels, which accelerate the convergence of the iterations within each time-step. In order to handle the large computational domain associated with wind turbine simulations, the domain decomposition approach is used to divide the total computational domain into multiple sub-domains. The sub-domains are computed in parallel with one processor-core per each sub-domain. This does not only make the computations faster, but also makes it possible to increase the resolution as more virtual memory is available when running on multiple processor-cores.

The spatial derivatives in the governing equations are discretized by first order upwind differences and second order central differences, of the connective and diffusive terms respectively. Third and fourth order accuracy are obtained for the convection and

diffusion derivatives respectively, by the use of defect-correction. This does according to Revstedt [17], ensure the stability of the lower order schemes and implies an accuracy of a higher order method, which is important to reduce numerical dissipation in LES. Second order accurate implicit scheme is used for the temporal scheme.

3.3 Turbulence

The majority of flows of engineering significance are turbulent. It is hard to make a strict definition of turbulence but it can, according to Tennekes and Lumley [24], be characterized by:

- random and irregular fluctuations
- three-dimensional and rotational in space
- dissipates energy to heat
- diffusive since the mixing rate increases
- property of the flow
- continuum phenomena

The *Reynolds number* (Re) is a dimensionless quantity of the relation between inertial and viscous forces in a flow defined as:

$$Re = \frac{UL}{\nu} \tag{3.5}$$

where ν is the kinematic viscosity, U and L are characteristic the velocity and length of the flow, respectively. This number is often used as a measure to determine whether a flow can be expected to be laminar or turbulent. Transition into turbulent flow occurs when the inertial forces increase compared to the viscous forces. Turbulent flows are thus expected at high Reynolds numbers. The limit of transition from laminar to turbulent flow is dependent on the choice of the characteristic parameters and the flow-case.
The turbulence in flows are distributed over different scales in both time and space. The spatial scale is related to the eddy-sizes. These sizes are limited by the geometric sizes of the flow-case in the higher range and the dissipation by viscous effects in the

lower range. In figure 3.1 is the turbulent kinetic energy distribution for turbulence at increasing wavenumbers visualized. The wavenumber is inversely proportional to the eddy sizes. The turbulent kinetic energy is produced mainly within the large scales. These scales are also containing the most energy, and is thereby the most important to resolve. Kinetic energy is in average transported from the larger to the smaller scales, as there is a net break down to smaller eddies. The transport takes place due to in-viscid effects over the inertial subrange and due to viscous effects over the viscous subrange, usually referred to as the *energy cascade*. The kinetic energy is finally dissipated into heat within the viscous subrange.

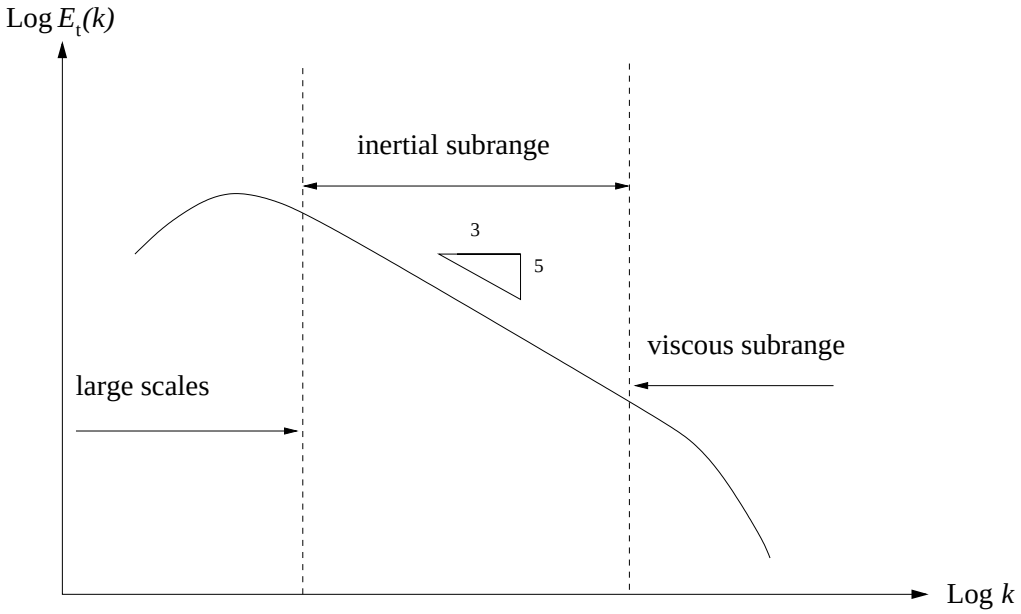

Figure 3.1: Turbulent energy spectrum. Density as a function of wavenumber k.

There are three main approaches of handling the task of resolving the temporal and spatial scales. The approaches are:

- *Direct Numerical Simulation* (DNS)
- *Large Eddy Simulation* (LES)
- *Reynolds Averaged Navier Stokes* (RANS)

The basic methods to achieve resolution are by either direct simulations or modeling. In DNS are all scales resolved by the numerical evaluation of the governing equations. Very high spatial and temporal resolution in the discretization is needed to achieve this, which demands extensive computational resources. DNS is, for this reason, impossible to use in most engineering flows, especially when a large domain is to be simulated.
LES involves a filtering process in which the large eddies are numerically simulated and the small ones are modeled by a *sub-grid scale* (SGS) model. Since the large scales contain the most energy, these can be expected to have the most influence on the flow. The small scales are, in contrary to the large scales, expected to have a universal behavior, thus making it possible to model them globally.
RANS simulations are achieved by averaging the governing equations in time before the numerical evaluation, and introducing a model for the influence of turbulence, e.g. the popular $k-\epsilon$ model. This approach is frequently used for engineering flows since the averaging in time significantly reduces the computational efforts as there is no need of averaging over transient solutions. It does however often fail to predict statistically unsteady phenomenas. Such phenomenas can be expected to appear in wind turbine simulations, where unsteady simulations are of great interest as the blades move. The modelling of turbulence within the large scales introduces poor physical representation since these scales depend upon the physical geometries associated with the flow. Large streamline curvatures and stagnation points are other characteristics of the flow, which can introduce errors in RANS simulations.
The approach used in the simulations of this project is LES, which is the method implemented in the in-house CFD-code. The SGS fluctuations are taken into account implicitly, as the third order upwind discretization scheme used for the convective terms acts dissipatively. This models the behavior of dissipation into heat in the viscous subrange, which has been shown by e.g. Ohlsson and Fuchs [16].

3.4 Virtual boundary method

One of the great challenges of full geometry wind turbine simulations is how to treat the solid boundaries, especially the moving boundaries of the blades. There are several different methods for treating solid boundaries in CFD. As one strive to achieve accurate physical representation of the flow along a solid surface, one has to consider the level of relevance, and computational effort needed to accurately represent the

boundary layer. A trade-off has to be made between the resolution of the boundary layer and computational feasibility. The aim is to sufficiently capture the influence of the boundaries on the large scale flow structures resolved in LES. This implies that the use of some kind of boundary modeling method is suitable. In section 2.3.2 there are two models mentioned, the actuator line and the actuator disc methods, employed by e.g. Ivanell [12]. Both of these methods have the advantage of representing the boundaries without the need of resolving the boundary layers numerically. The disadvantage is however that both methods rely on empirical data representing the influence of the geometries on the flow.

The method previously implemented in the in-house CFD code, and employed on wind turbine simulations by Szasz and Fuchs in e.g. [23], is the *virtual boundary method*, also referred to as the *immersed boundary method*. This method rely on source terms added to the momentum equations. These represents the boundaries by iteratively introducing a force to the nodes adjacent with the boundaries until the velocity at the boundary has converged to the correct value. The method is suitable for cartesian grids, which has the disadvantage of not being possible to fit to complex geometries unlike unstructured grids. Unstructured body-fitted grids does however demand considerable computational efforts in comparison with cartesian grids, and introduce difficulties in handling moving boundaries. The moving boundaries can be represented in the virtual boundary method since the target velocity at the boundary can be set to an arbitrary value. In this case the velocity is set to the product of angular velocity and distance from the rotor center. The method should thereby sufficiently capture the flow surrounding the full geometry of the wind turbine without demanding too high computational efforts.

Chapter 4

Design and Set-up

The wind turbine design and it's implementation in the CFD-simulations will be described within this chapter. The set-up of the computational domain and the different cases will also be presented.

4.1 Wind turbine design

The geometry will be described within two subsections, one describing the rotor and one describing the stationary part, which consists of the tower and nacelle.
The overall design is a 1.86 MW mechanical power horizontal axis wind turbine with a rotor diameter of 78 meters and a hub height of 58.5 meters, seen in figure 4.1. The dimensions can represent a quite small offshore wind turbine with the measures given today. The rotor diameter has been used for normalization, whereby 78 meters correspond to 1 spatial-unit in the following descriptions. All of the solid bodies are treated by the virtual boundary method in the simulations, which is described in section 3.4.
The wind turbine geometry-files used in the simulations have been generated by a Fortran program, written by the author in the course of this degree project. The program creates a full wind turbine geometry from specified dimensions and airfoil data.

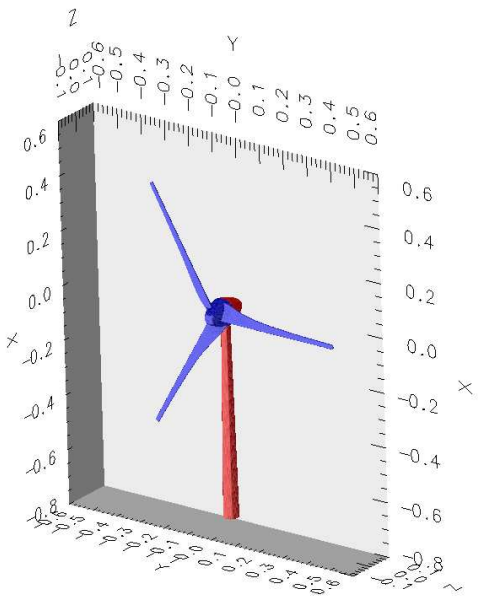

Figure 4.1: Wind turbine design

4.1.1 Rotor

The rotor consists of three blades and one hub. The hub geometry is described by the simple shape of a parabola revolved around the rotor-axis. There is a range of different blade geometries used within the industry, which are designed for different operational conditions. The geometries used within the industry are, however; difficult to access, and the scope of the performed investigation makes it more or less sufficient with a realistic blade geometry rather than one in operation. The blade geometry used in the computations has has been developed by Mickaël Edon, and has been presented in an internship report [10] carried out at Nordic Folkecenter for Renewable Energy in Ydby, Denmark. It has been derived from two-dimensional airfoil data with the program WRD.

The blade-geometry is based upon one single airfoil called FX 66-S-196 V1. This airfoil provides a high lift to drag ratio and has been evaluated by e.g. Bertagnolio et al. [5]. Along the length of the blades there are variations in both chord length and twist (quantified in appendix A). The chord length decreases from about 4.3 meters at the root to 0.85 meters at the tip. Reference point for the twist is the tip position, which is parallel with the plane of rotation at zero pitch angle. The blade geometry is illustrated in figure 4.2

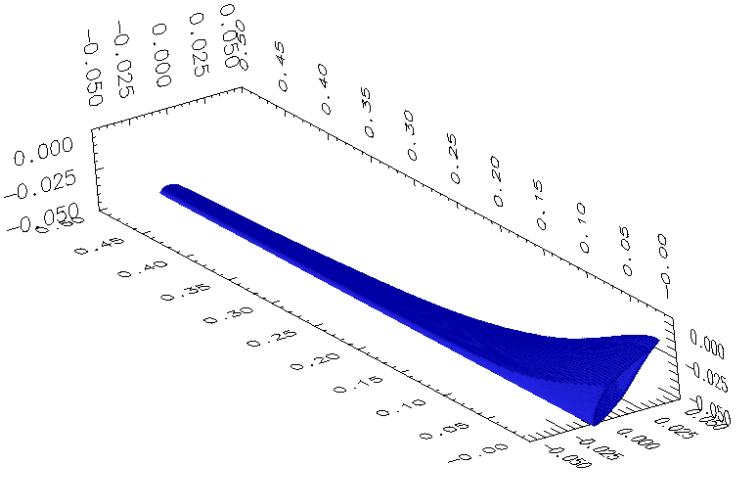

Figure 4.2: Blade geometry

Commercial blades are most often a combination of different airfoils along the blade, where each profile is optimized for the oncoming wind speed prevalent at a certain radius. This indicates that the single profile blade used within the computations is not fully optimized. Details on the estimated performance of the rotor, carried out by the BEM program WRD, are shown in section 2.3.3.

4.1.2 Tower and nacelle

The geometry of the tower has the shape of a tube with a linearly decreasing radius from the bottom to the top. The radius at the top is half the bottom radius. There are a couple of different types of nacelle geometries available within the market of wind turbines. The one used within this project have the shape of a revolved parabola, similar to the geometry of the hub, but longer. This was chosen because of its simplicity and quite good aerodynamics compared with box-shaped types. Since the influence of nacelle geometry is not of specific interest, it should be desirable to use a nacelle that can be expected to have a low influence on the flow.

4.2 Atmospheric boundary layer

The atmospheric boundary layer imposed on the oncoming flow in the simulations is a simplification of the actual conditions prevalent for real wind turbines. The wind is in reality fluctuating with time, but have been modeled as a constant average over time with variations in vertical direction due to the ground-friction. The boundary layer is described by the following power law wind shear profile:

$$w(x) = w_{hub}\left(\frac{x}{x_{hub}}\right)^{\beta} \tag{4.1}$$

where w is the axial velocity, w_{hub} the axial velocity at hub height, x the vertical position, x_{hub} the hub position and β Hellmann's exponent, set to 0.15 in accordance with simulations performed by e.g. Ivanell [12]. The interested reader is referred to [26] for further descriptions on atmospheric boundary layers. The axial velocity at hub height, w_{hub}, has been set to 10 m/s. This value has also been used for normalization, thereby corresponding to 1 velocity-unit.
The conditions are comparable with the ones prevalent at offshore sites where the turbulence intensity is low and no obstacles are interrupting the oncoming flow.

4.3 Operating characteristics and cases

Two main cases have been studied, both consisting of two wind turbines in a row, as shown in figure 4.3. The two cases differ by different pitch angles for the first wind turbines. A reference case with one wind turbine has also been set up and used for evaluation of the basic characteristics of the wake. The operating characteristics and notations of the cases are presented in table 4.1.

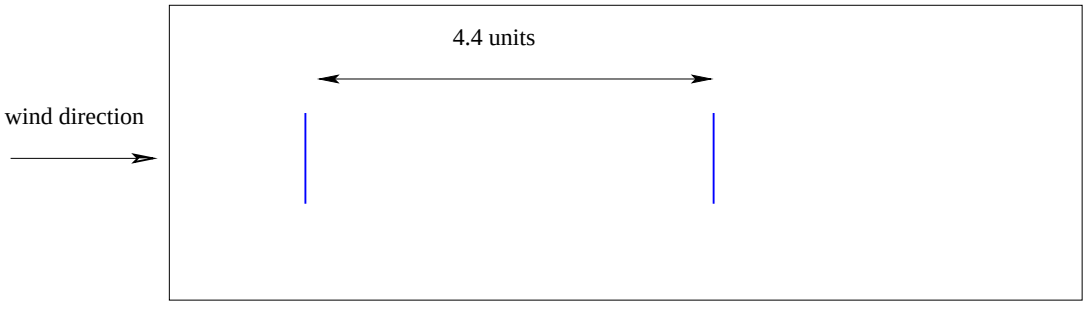

Figure 4.3: Set-up of two wind turbines (shown as lines), seen from above.

Table 4.1: Cases and operational characteristics

Case		1st WT	2nd WT	
number	notation	pitch angle	pitch angle	TSR
1	-0.9 deg. pitch	-0.9 °	-0.9 °	9.2
2	9.1 deg. pitch	9.1 °	-0.9 °	9.2
3	single WT	-0.9 °	-	9.2

4.4 Computational domain

The spatial domain in the computations is the volume for which the flow field is evaluated. The volume has to be limited since every unit of volume require computational efforts. Flow past immersed boundaries thus imply that the real volume of fluid has to be modelled within the finite dimensions of a domain. Furthermore, all CFD-simulations require measures needed to account for the properties at the boundaries of the domain, in order to evaluate the numerics. The properties at the boundaries are called boundary conditions. The numerical approach also require, as described in 3.2, a discrete representation of the domain, which is achieved with a mesh within the volume. The following sections will give more details on boundary conditions and mesh used within the simulations, whereas the spatial and temporal domains will be described bellow.

The total spatial domain consist of multiple sub-domains. The sub-domains can then be computed in parallel by one processor each, thus significantly decreasing the computational time required. The geometry and dimensions of one sub-domain can be seen in figure 4.4. Both sub-domains with and without a wind turbine has been used, as can be seen in figure 4.5, where the set-up with two wind turbines is illustrated. The interfaces between the sub-domains are overlapping by four cells, which is why the total length of the full domain is less than the length of all sub-domains. The overlapping is needed for the communication between the sub-domains in the parallel computations.

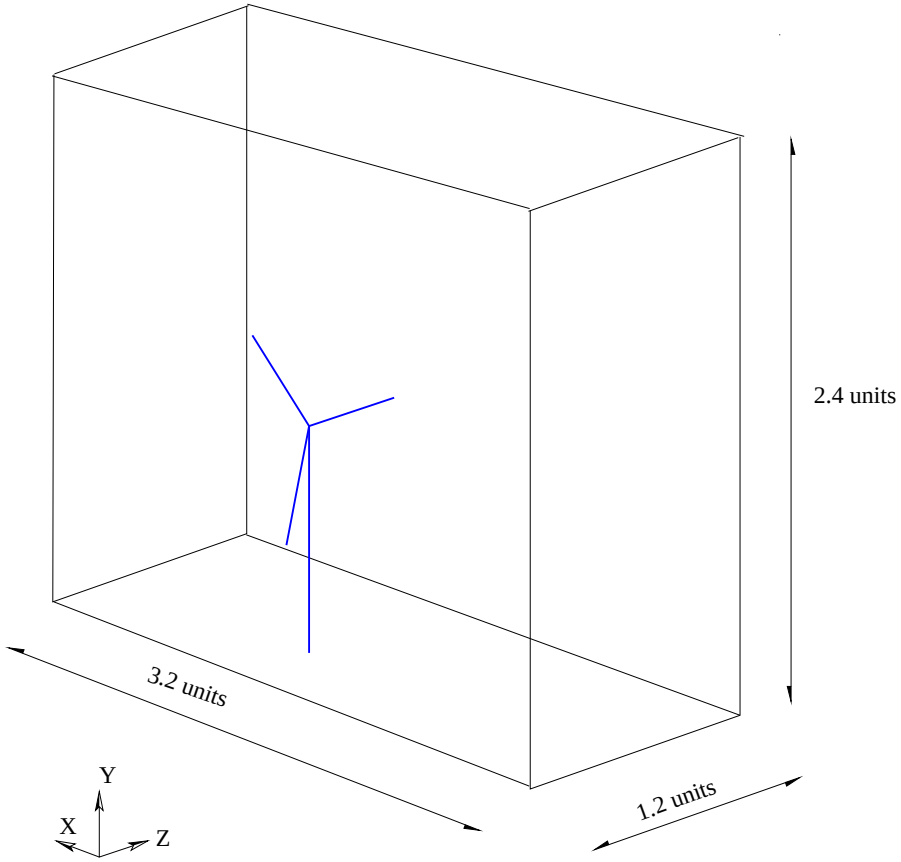

Figure 4.4: Sub-domain with dimensions.

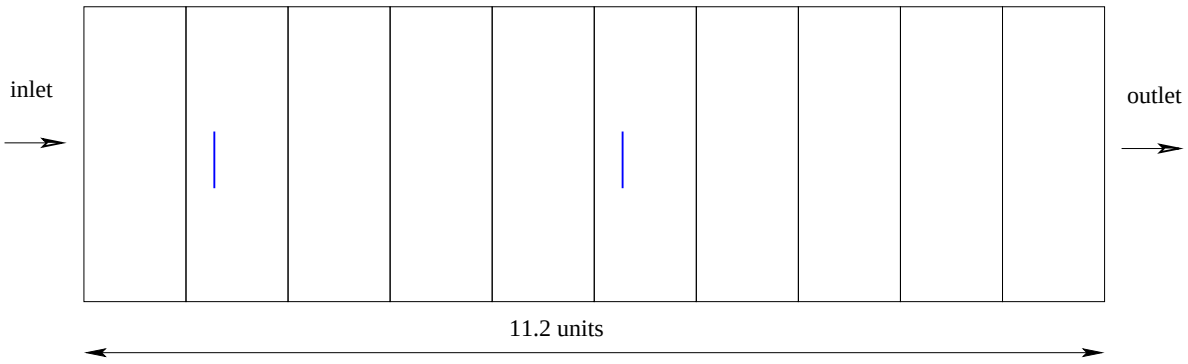

Figure 4.5: Full domain illustrated from above with 10 sub-domains and two wind turbines (shown as lines).

The time step in the simulations has been 0.003 seconds, which gives a *Courant-Friedrichs-Lewy* (CFL) number of approximately 0.56. The CFL number describes the relation between the travel distance of a fictive particle in the flow and the time-resolution, and is formulated as:

$$C = \frac{\Delta t U_{ref}}{\Delta x} \tag{4.2}$$

where Δx is the distance between two nodes in the mesh (described in section 4.4.1) at the highest resolution, Δt is the time-step and U_{ref} is a reference velocity of the flow, preferably the highest prevalent in the flow. In this case the tangential speed at the tip of the rotor blades has been chosen as U_{ref}, however higher velocities can exist in the flow, e.g. in the tip vortices. The CFL number is an indication on whether the characteristics of the flow is possible to capture with a certain time-step and mesh. Since the time-marching scheme in the CFD-code is implicit, there is no strict limit of the CFL number. It can, however be used as a measure of the relation between resolution in time and space. The choice of time-step is a trade-off between sufficient resolution in time and the computational time. Comparisons have been made between simulations by varying the time-step, yielding CFL numbers of 0.56 and 0.28. No significant differences were observed, verifying that the higher CFL number is sufficiently low.

4.4.1 Mesh

The mesh used within the simulations is cartesian and equidistant, with one refinement region in each sub-domain, in the vicinity of the wind turbine. The length between two nodes is 0.0125 in the global mesh and 0.00625 units in the refined region. This yield a total number of about 7.3 million nodes per each sub-domain. Coarser global grids are also prevalent since the multi-grid method is used. There is three levels of coarser grids based on the global grid.

4.4.2 Boundary conditions

The boundary condition for the velocity components at the bottom plane is set to zero, representing the stagnation along the ground and the impermeability across it's surface. Along the sides and top of the domain, the zero-gradient boundary conditions is used for the velocity components parallel with the boundary. This is representative

for a flow where the boundaries are sufficiently far away from any disturbances, thus possible to assume that the changes across the boundary are negligible. The velocity component perpendicular to the boundaries at the top and sides is set to zero. This condition is the most suitable since the main flow direction is parallel with these boundaries. It also simplifies the approach for ensuring mass conservation.
The inlet boundary of the domain (seen in figure 4.5) has the boundary condition defined by the atmospheric boundary layer profile, described in section 4.2. The outlet boundary has the boundary condition zero gradient for all velocity components. This is valid if the outlet is sufficiently far away from the formation of the wakes, making it possible to assume that the variations in the flow field are negligible across the boundary. The flow field at the outlet is also treated by a correction function which ensures that the mass-flow at the inlet equals the one at the outlet, thus fulfilling mass conservation.

Chapter 5

Results and Discussion

The results from the simulations will be presented and discussed within this chapter, from which conclusions later will be drawn. The first results to be presented are dealing with the influence of pitch control. Subsequently the strengths and weaknesses of the simulations will be further analyzed from different aspects.

5.1 Influence of pitch

Figure 5.1 shows an overview of the two cases and the averaged axial velocity. An iso-surface of zero axial velocity is shown to illustrate the proportions of the recirculation zones. It is possible to identify a small difference in recirculation, after the first turbines, between the two cases. The case with -0.9° pitch has a less tapered shape, which indicates more extensive recirculation since the zones have the same length. The recirculation is dependent on the rate of power-extraction from the flow, and higher recirculation can be expected if the power extraction increases. This result corresponds with the expected drop in power with increased pitch angle. From figure 5.1 it is, however, not possible to identify any significant differences in recirculation behind the down-stream turbines.

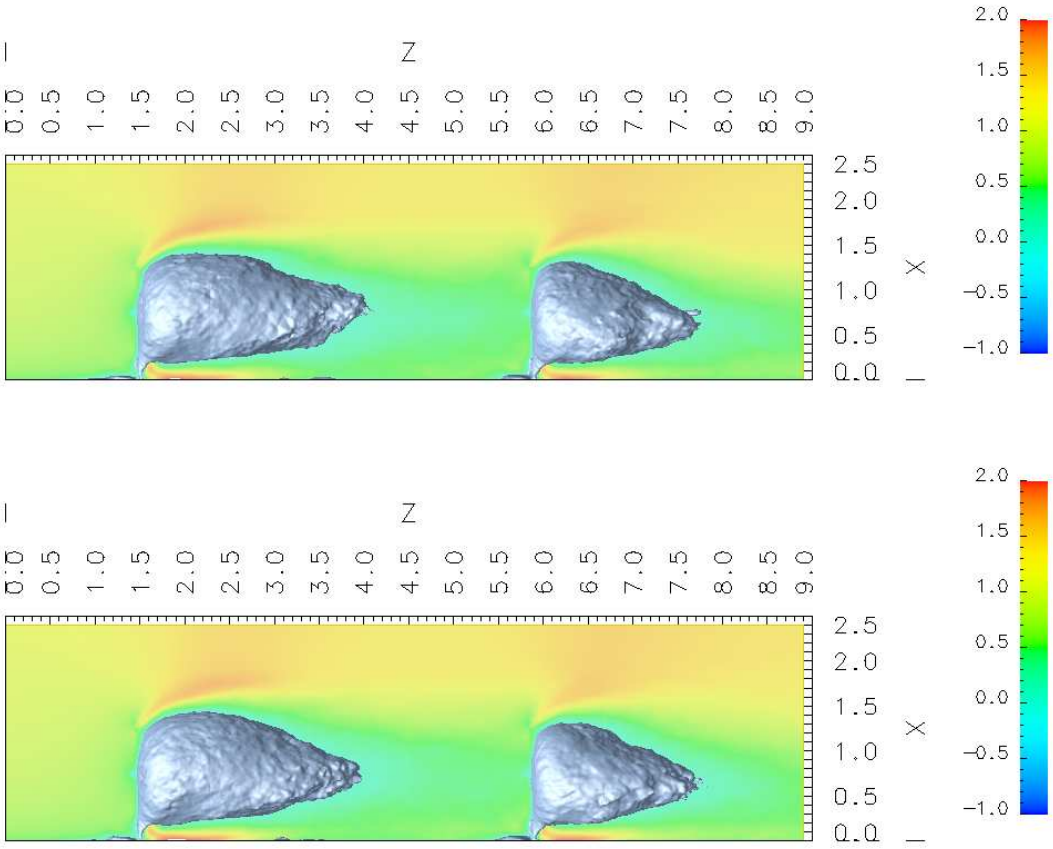

Figure 5.1: Vertical plane with averaged axial velocity, iso-surface at zero velocity. -0.9° pitch (upper) and 9.1° pitch (lower).

The kinetic power within the flow has been evaluated over a circular area parallel with the rotor plane according to the following equation:

$$P = \int_A \Big(\frac{1}{2}\rho v(x,y,z)^3\Big) dA \tag{5.1}$$

where v is the velocity magnitude, ρ is the density and A defines the area of the disc to be integrated. This equation is in accordance with the basic strategy to evaluate extracted power by the variation in kinetic energy, used in the derivation of Betz's limit, seen in e.g. [14]. The quantity has been normalized with the kinetic power at the inlet of the domain, and plotted in figure 5.2 along the axial direction. This measure is here denoted *power ratio*, since it describes the rate of power left within

the radius of the disc, at a certain axial position.
Between the axial positions 0 and 3.5 in figure 5.2, one can see that the lines from the two cases are practically over imposed. The sudden jumps at axial positions 1.5 and 5.9 are due to the virtual boundary method, implemented to account for the solid bodies. The flow inside the bodies is not physical and contaminate the integrals at these axial positions. Moving downstream the first wind turbine, the two lines are over imposed for approximately 0.5 units. This region is affected by the radial expansion of the wake, which is larger than the integrated area. The peripheral flow, which is expected to contain a high amount of the energy in the wake, is not captured within the integrated area in this near-wake region, thus under-estimating the power ratio. From about two units downstream the first turbine more realistic behavior of the wake is shown, and the differences between the cases also appear. These tendencies correlate with the expected decrease in power extraction with increased pitch angle.
The power extracted by the second wind turbines does however not seem to differ significantly, given the oncomming difference. According to Ivanell [12], the wake re-energization length should be much shorter behind the second turbine than the first, due to higher turbulence intensity contributing to the breakdown of vortices. This phenomenon is shown, but obviously at a too high extent. The power ratio behind the second wind turbine is expected to decrease, but does not. The reasons for this might be found in both the evaluation method and the physics of the results. The physics of the results might be compromised by a too small cross-section perpendicular to the axial direction, which will be further discussed in connection with figure 5.6. It has, from the single wind turbine simulations, been possible to verify that the wake length is not affected by the outlet boundary condition.
One can also reflect upon the quantitative difference in power ratio behind the first wind turbines, which is quite small considering the significant difference in pitch angle. Comparisons can be made with the data presented in table 2.1, where a pitch increment of 2° at a wind speed of 11 m/s gives a drop in power of about 8%. The maximum difference, shown at axial position 5 for the simulations, is about 6%, with a pitch angle of 10°. It should be emphasized that both results originates from simulations, which limits the possibilities of drawing any quantitative conclusions, thus only showing indications.
It is further more possible to conclude that the large variations in power ratio makes it difficult to evaluate a uniform power coefficient corresponding to the one formulated

in equation 1.1. The method is also sensitive to the choice of diameter of the disc, which will be discussed within section 5.2.

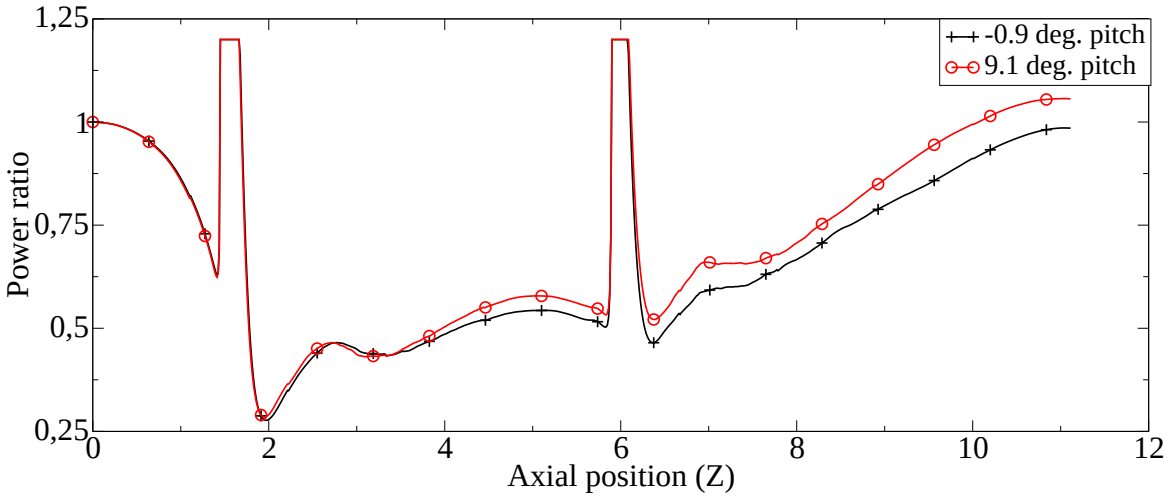

Figure 5.2: Variation of power ratio along axial direction in a circular plane perpendicular to the axis (diameter of 1.5 times the rotor diameter).

In figure 5.3 the time averaged axial velocity is shown from above. It can be seen that the the flow is not symmetric along the axis, which has an effect on the validity of the power ratio evaluation method. The non-symmetric wake distribution introduces higher velocities within the area of the discs, from which power ratio is evaluated, thereby increasing the power ratio. This might explain the gradual increase seen in figure 5.2 from the axial position 7. Since the non-symmetric behavior is present in both of the cases it should however not influence the possibilities of comparisons. The asymmetric behavior might occur due to low frequency phenomena such as wake meandering. More results on wake meandering are presented in section 5.3.
One striking characteristic of the results is the large recirculation zone seen in both figure 5.1 and 5.3. From the latter it is also possible to conclude that high negative axial velocities occur within the wake, contributing to the large wake expansion close to the rotor plane. These features will be further evaluated within section 5.4 where the formation of the wake will be investigated.

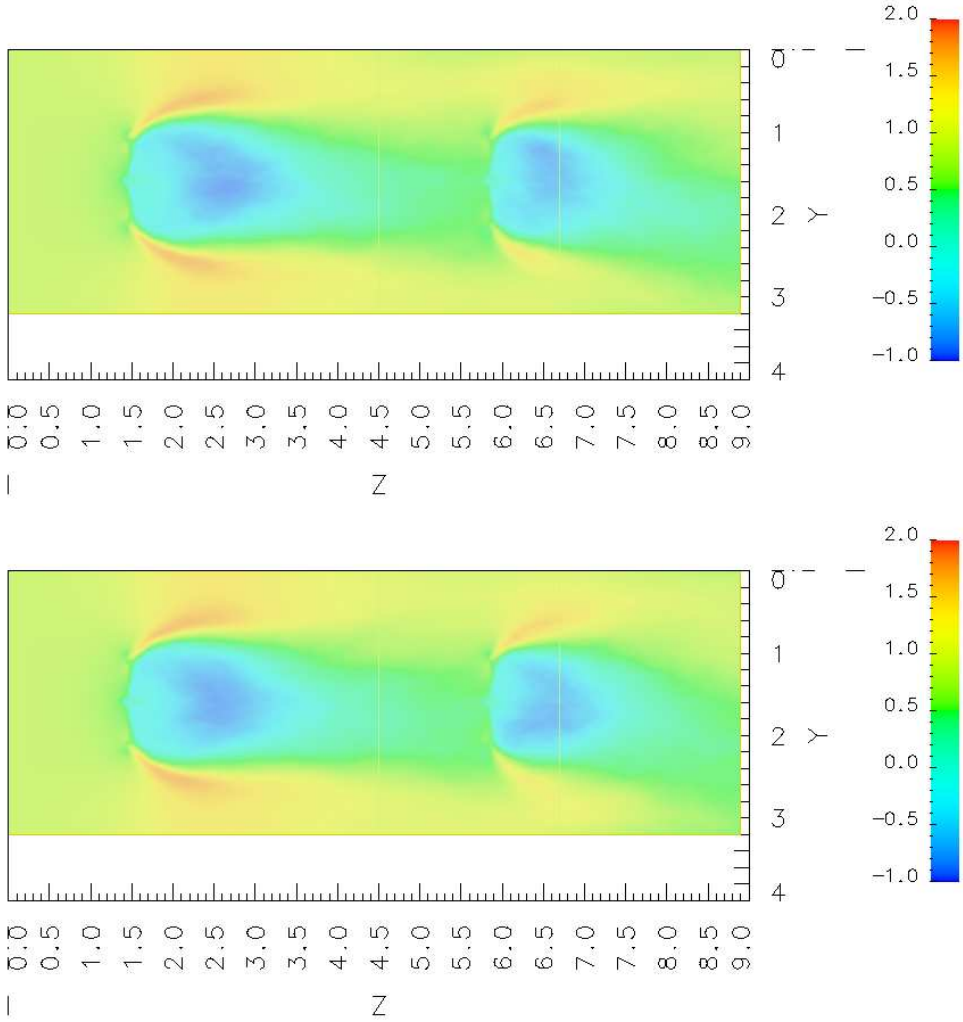

Figure 5.3: Horizontal plane with averaged axial velocity. -0.9° pitch (upper) and 9.1° pitch (lower).

The axial velocity, and thereby the recirculation, is quantified along the flow direction in figure 5.4. Since the data is taken for a line going through the rotor center it can be expected to capture the highest negative velocities present in the flow field. The stagnation points at the hub positions are clearly visible. The velocity decreases monotonically for over 0.5 units and recover to zero velocity at about the same length. These characteristics are evidence of a recirculation zone resembling the one illustrated in figure 5.5. The tendencies in the figure indicate that the axial velocity recovers faster with increased pitch. The differences are however small.

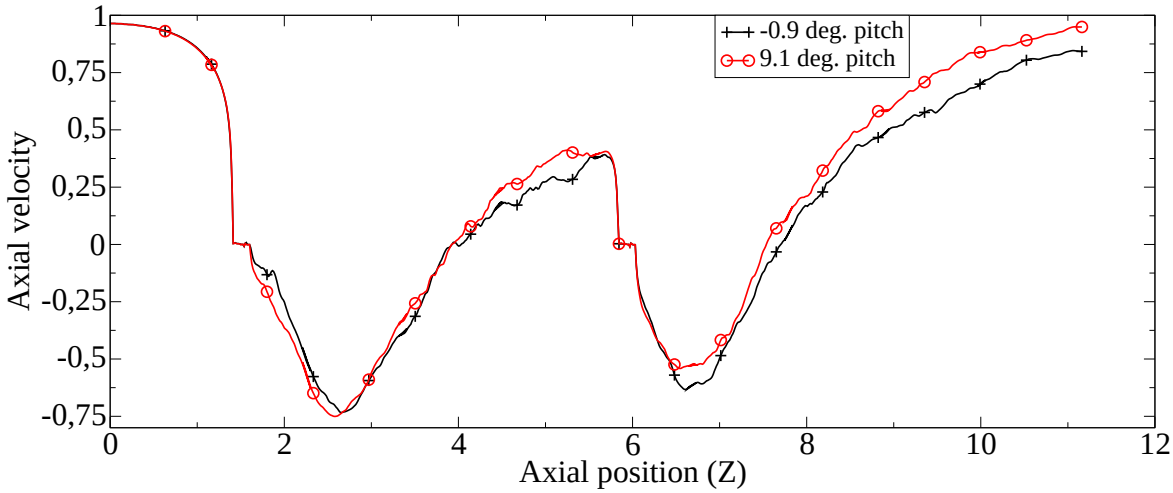

Figure 5.4: Variation of averaged axial velocity along axial direction through rotor center.

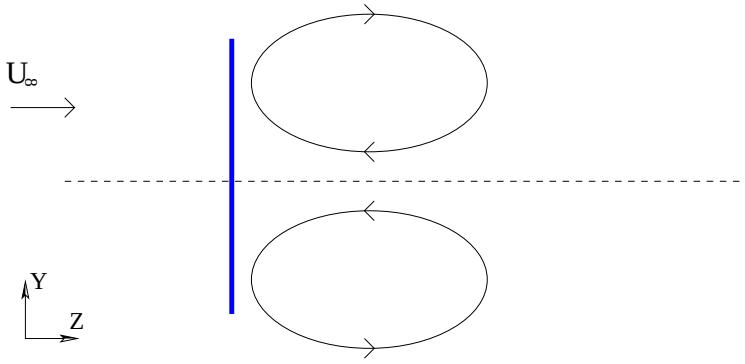

Figure 5.5: Illustration of the recirculation zone occurring behind the wind turbines, seen from above.

In figure 5.6 the axial velocity along lines at 2.7 units behind the wind turbines is shown for both cases. It is possible to see that the reduction in axial velocity behind the first wind turbine is less for the case with increased pitch. This is also the case behind the second wind turbine, which is not unexpected if the oncoming wind speed is higher. The difference is concentrated at the rotor center, which further indicate that the structures of recirculation are dominating the wake and increase in magnitude with increased power extraction.

For the first wind turbines, one can see a quite small displacement in Y-direction, of the wake. The displacement seems to be amplified behind the second wind turbine, where it reaches almost 0.5 rotor diameters. The unsymmetric behavior seen in the results will be discussed further in section 5.3.
The velocity profiles behind the second wind turbines indicates that the second wake is wider than the first. Further more, it should be considered whether the in- and outlet boundary condition on mass-conservation through the domain influences the width of the wakes. Figure 5.6 indicate that this might be the case for the downstream wind turbines. Mass-flow is only let through the boundaries at the in- and outlets of the domain. If the cross section is too small in relation to the obstruction, increased flow, thus higher velocities, will be forced along the boundaries. This can both decrease the wake expansion and force re-energization of the wake in an unphysical manner. The high recirculation and large wake expansion, leading to a large obstruction of the flow, was not anticipated in the set-up of the cases. It is however from figure 5.6 evident that a larger cross-section of the domain should have been used to ensure that the flow is not too much affected by the boundary conditions.

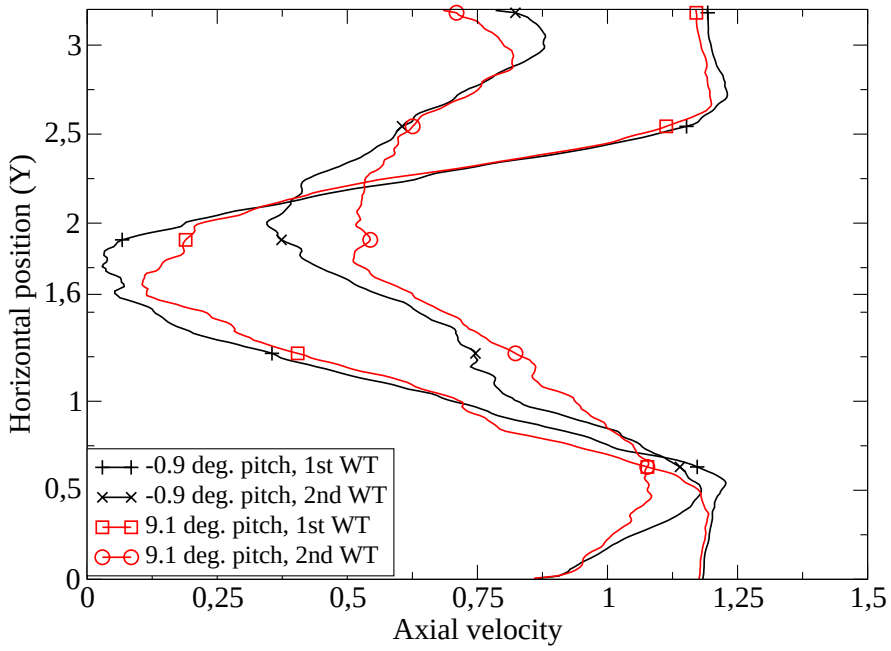

Figure 5.6: Variation of averaged axial velocity along horizontal lines 2.7 rotor diameters behind the wind turbines at nacelle height.

The time averaged RMS fluctuations are illustrated in figure 5.7, showing turbulence originating from the tips and low turbulence at the root regions. The figure also shows indications of two centers of recirculation behind the rotor, similar with the ones illustrated in figure 5.5. As described by Medici [15], heavy loading of a wind turbine will result in a large back flow region behind the rotor as the wake enter the turbulent-wake state.

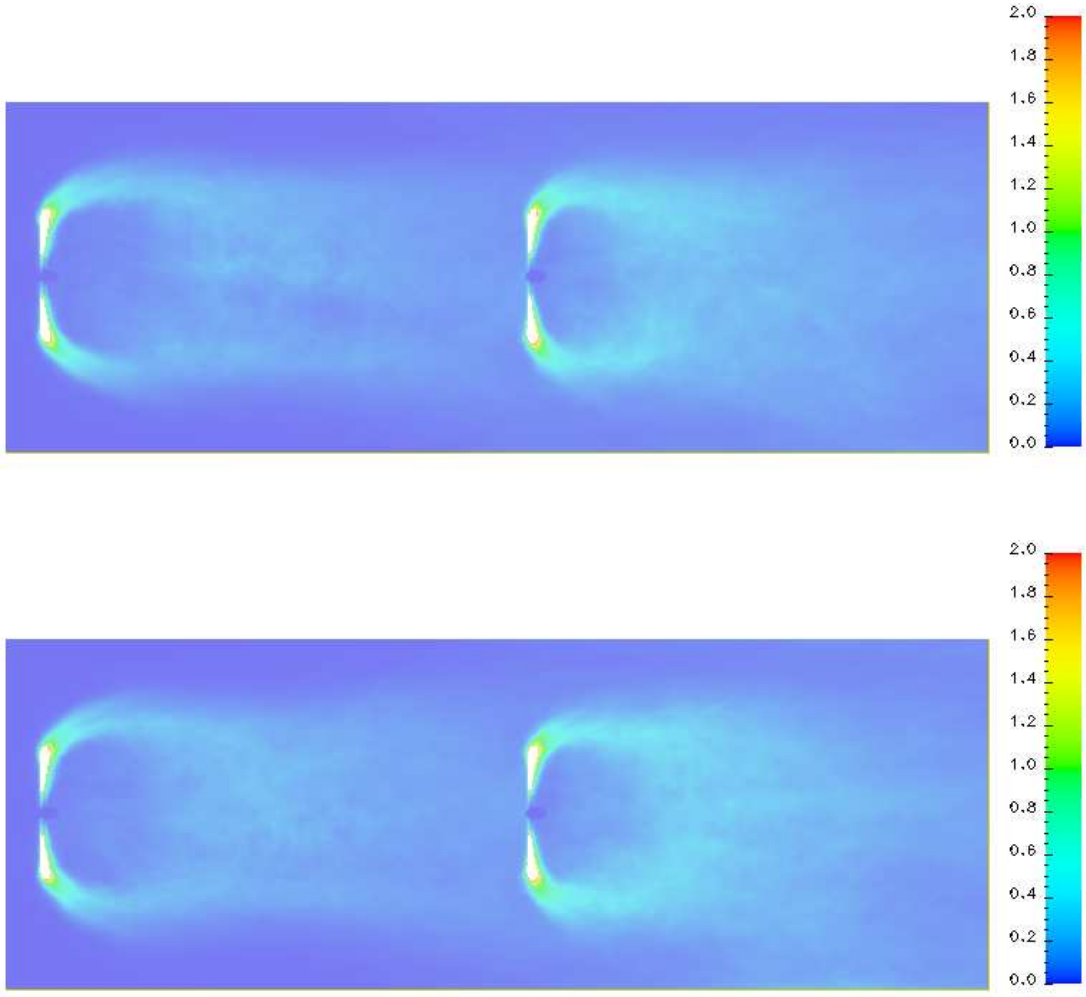

Figure 5.7: Averaged RMS variation of total velocity in horizontal plane. -0.9° pitch (upper) and 9.1° pitch (lower)

The fluctuations are further quantified in figure 5.8, where the time averaged RMS variation has been plotted along lines behind the turbines. The level is slightly higher toward the center of the rotor in the case with increased pitch. It is also possible to see that the rate of fluctuations is higher and more evenly distributed behind the second wind turbines. The level is also slightly higher at the tip positions in the case with increased pitch. This indicates higher losses due to tip-vorticies, which is expected if the total rate of power extraction increases.

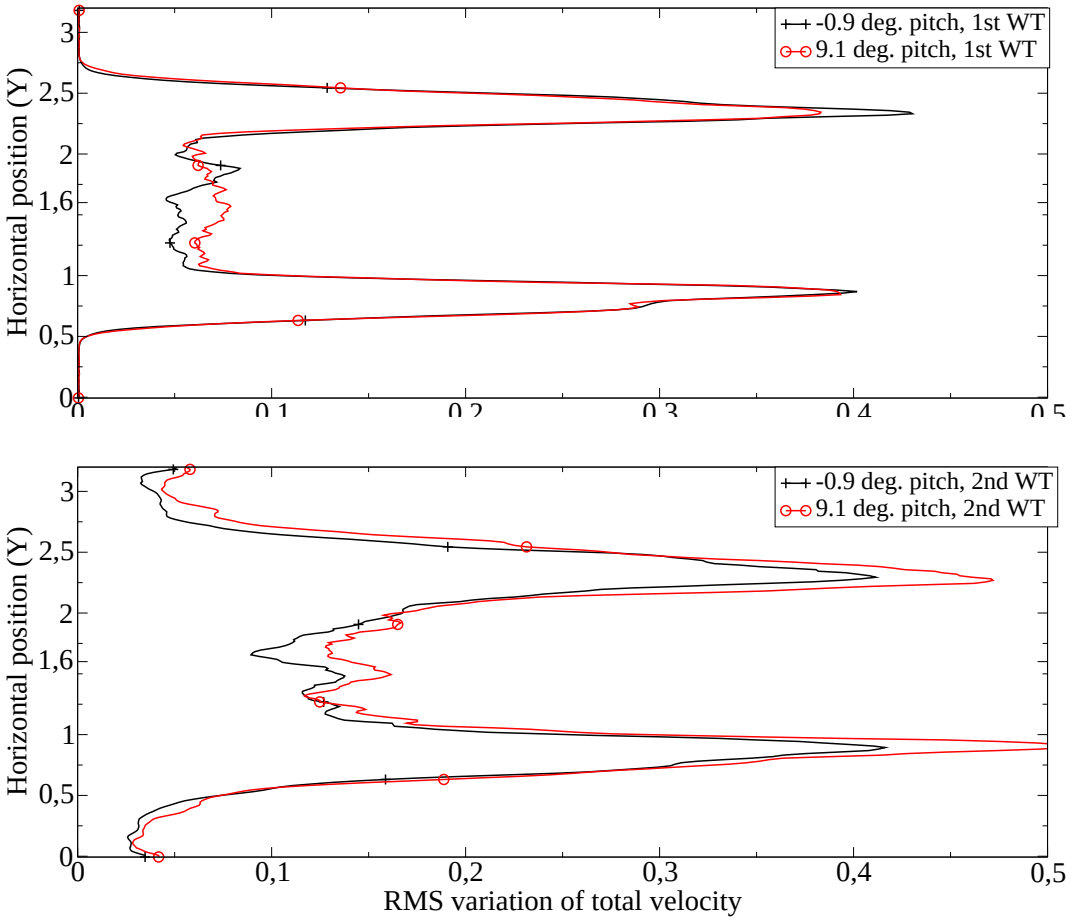

Figure 5.8: Averaged RMS variation of total velocity along horizontal lines behind first (upper) and second (lower) wind turbines.

5.2 Power-ratio evaluation method

The evaluation of the extracted power has to be made from the flow-field since the CFD-code does not have any method implemented for evaluating the rotor torque. The power ratio evaluation method has to be carefully considered in order to justify the conclusions drawn from it. The difficulties are connected to the complexity of the flow field and the choice of region to evaluate. Hence the influence of disc area will be presented and discussed in this section. Results from the reference case with a single wind turbine have been used.

The power ratio is plotted in figure 5.9 for four different disc diameters, of which three are constant values at 1, 1.5 and 2 times the rotor diameter. The radius of the fourth disc is a function of the mass-flow, which is kept constant. This results in an increased disc diameter as the axial velocity decreases when passing the wind turbine. The approach thus shares the principles of a stream tube with the actuator disc method described in section 1.2.2. From the three plots with constant radius, one can conclude that the lowest and highest radius seems to over and under predict the power extracted respectively. The over prediction can be expected since the increase in velocity due to tip vortices is not captured within the small radius. The under prediction for the largest radius is due to the fact that the power extraction is too small, relative to the oncoming kinetic power, which is used for normalization. In an attempt to avoid the necessity of choosing one single diameter, the approach with variable radius, as a function of constant mass-flow was implemented. From figure 5.9, it is however possible to conclude that this method is not suitable for quantative evaluation of the power extraction since a stable value is not reached until much too far behind the turbine. The wake has then been re-energized from the free stream flow before reaching a stable value, and the method does therefore under predict the real power extraction. This characteristic makes the method unusable for evaluation of turbines placed in a row since the space between the turbines then is too small. The large variation of disc diameter, which can be seen in figure 5.10, is due to the high recirculation. Further more, at diameters above 1.5 units, the disc will not be circular because of the nacelle height of 0.75. One should also reflect upon the validity of the assumptions one has to make in a stream tube approach. The assumption of axial symmetry is probable to introduce errors, which has been discussed in connection with figure 5.3 in section 5.1.

The conclusion on which method is the most suitable to use turns out to be a constant

diameter large enough to capture the expansion of the wake, but not larger than the nacelle height. The diameter of choice is then 1.5, and it should be emphasized that this measure is only suitable for comparisons between cases and not for quantitative

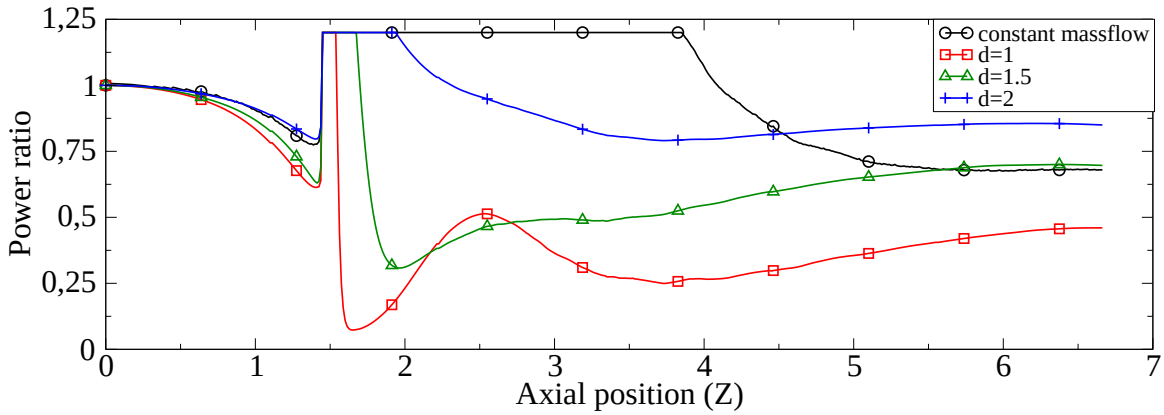

Figure 5.9: Variation of power ratio along axial direction in a circular plane perpendicular to the axis with different disc diameters. Single wind turbine

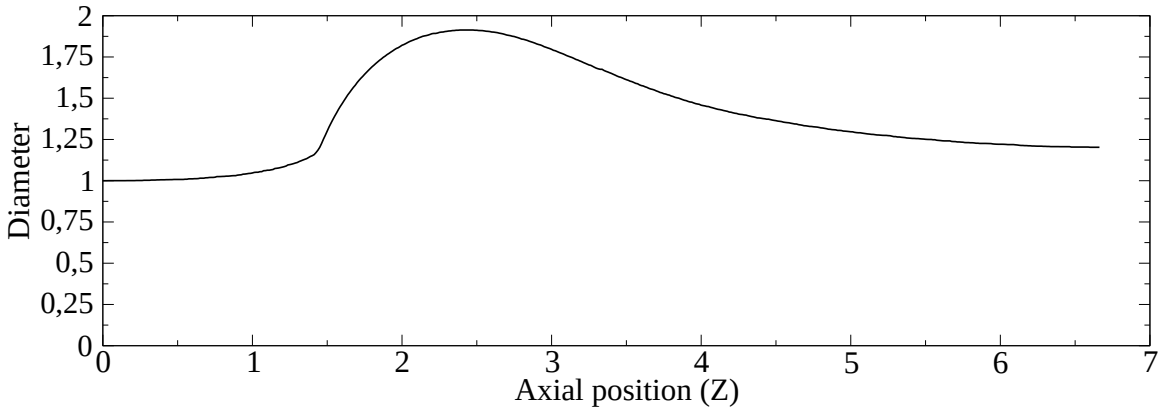

Figure 5.10: Variation of disc diameter as a function of mass flow along axial direction. Single wind turbine

5.3 Wake meandering

Unsymmetric behavior can be expected since the set-up is not entirely symmetric. It is also probable to occur because of wake meandering, described in section 1.3.2, which according to Medici [15] will be present at high tip-speed ratios. The meandering effects should however, not be present in averaged results, as previously indicated in figure 5.3. The phenomenon is ideally symmetric in space over time. This does however require that the period to sample the average is long enough in relation to the period of the phenomena. The non-symmetry of the setup is a consequence of the direction of rotation, tower, domain boundaries and atmospheric boundary layer of the free stream flow.
Indications of wake meandering can be seen in figure 5.11 where the instantaneous axial velocity is shown for three snapshots taken with an interval of ten rotor rotations. Here one can see that the wakes move in both positive and negative Y-direction.

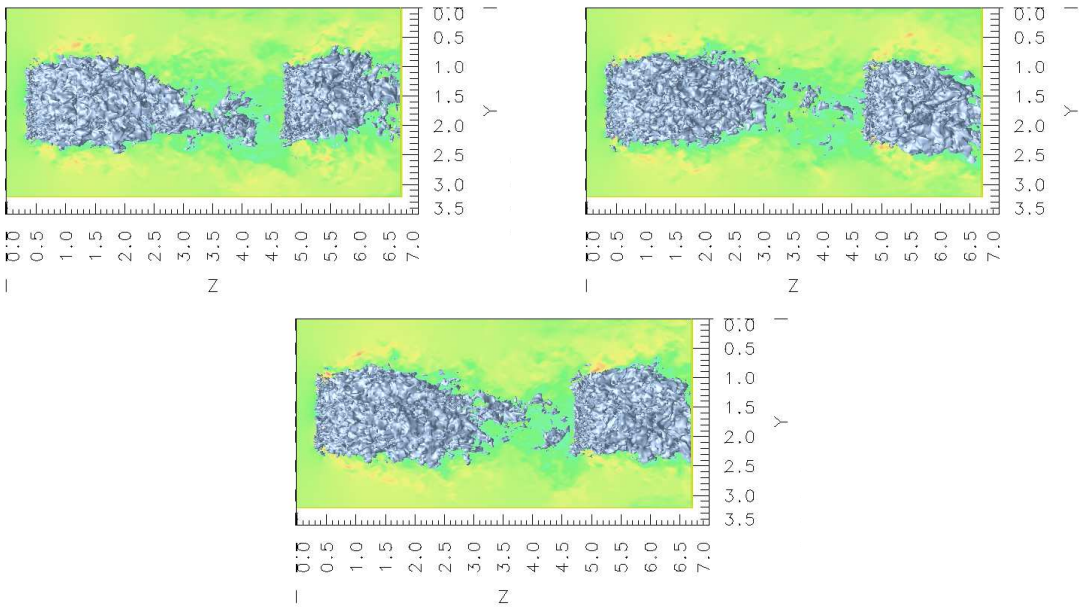

Figure 5.11: Horizontal plane with instantaneous axial velocity at three moments with 10 revolutions between each, iso-surface at zero velocity. -0.9°pitch.

Figure 5.12 illustrates how the axial velocity varies over time along a horizontal line at a distance of 4 units behind the first rotor. One can conclude that there are significant variations perpendicular to the rotor axis. It is not evident which

frequencies are dominant, only possible to conclude that there are low frequencies prevalent. Filtered versions of the figure are shown in appendix B.

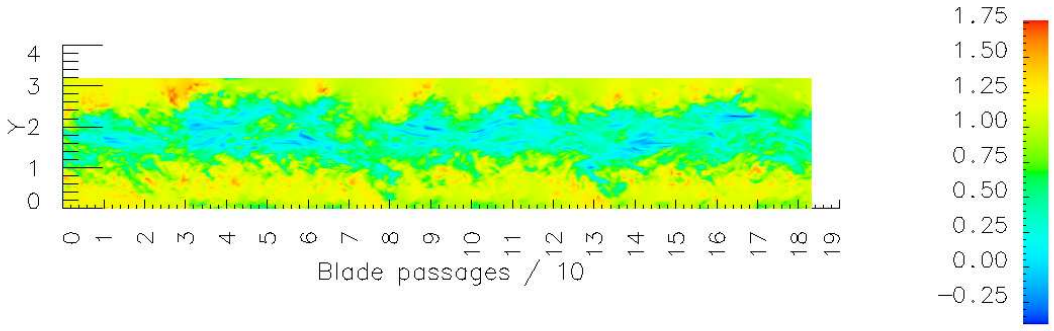

Figure 5.12: Axial velocity over time along a horizontal line 4 units behind the first rotor. -0.9°pitch.

In figure 5.13 one can see the variation of the three velocity components over time, and the energy spectrum visualized through a *discrete Fourier transform* (DFT). It is from this picture possible to verify the difficulties of determining a dominant frequency of the wake meandering motion. The sampling duration has to be considered in order investigate whether it is possible to capture such low frequency phenomenas. The expected frequency of wake meandering can be estimated through a Strouhal number of 0.12 (clarified in section 1.3.2) for high tip-speed ratio turbines. By equation 1.5 an estimated wake meandering blade passage frequency of 0.014 is given. This corresponds to a period of 70 blade passages, which can not be sufficiently captured within the present sampling duration of 180 blade passages. The energy spectrum does however show a low frequency peak, at the blade passage frequency 0.02, which is within the same order of magnitude as the estimated frequency. The short sampling duration, compared with the low frequency phenomenas, can thus be concluded as a possible reason for the unsymmetrical behavior of the averaged results.
Wake meandering introduces a not insignificant need of longer time duration of sampling to resolve all time-scales accurately. The consequences of this will be further discussed and analyzed in section 5.6. It should also be of interest to evaluate the influence of domain size perpendicular to the flow since these domain boundaries might influence the motions of wake meandering.

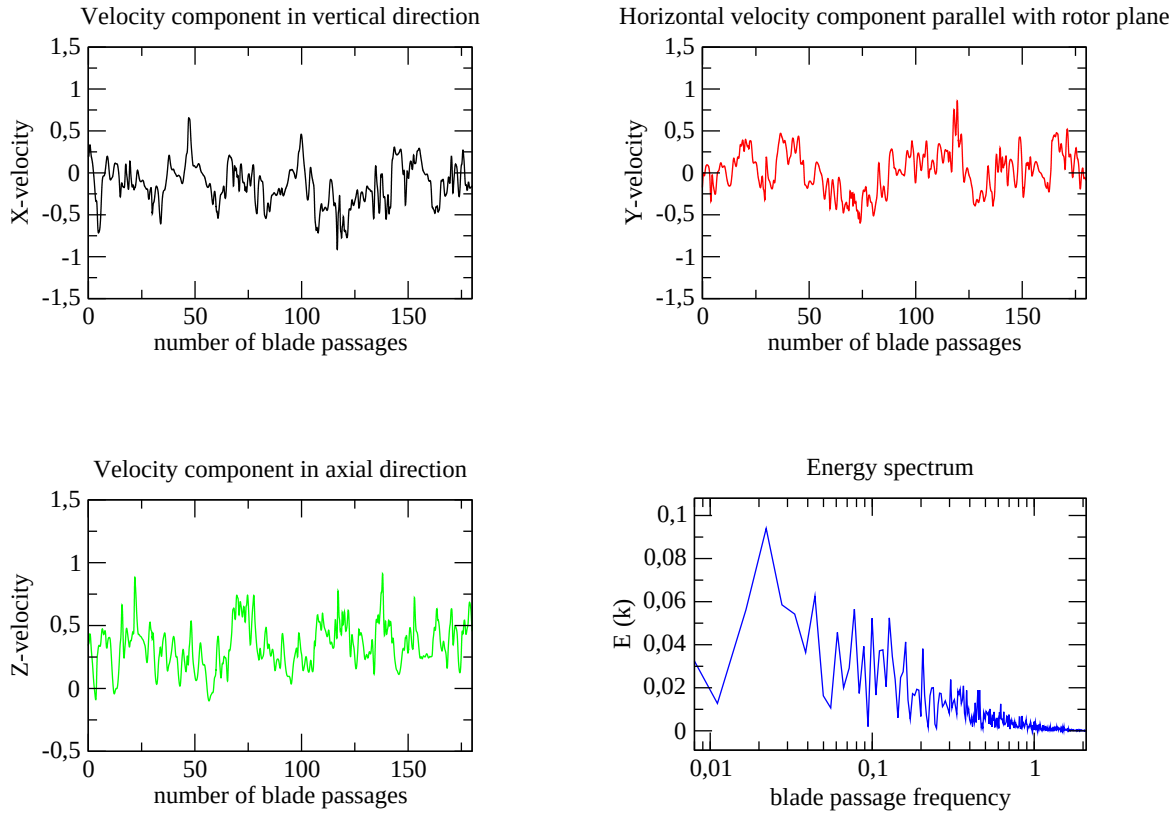

Figure 5.13: Velocity components and energy spectrum over time at hub height, 4 units behind the first rotor. -0.9° pitch.

5.4 Near-wake characteristics

Trailing vortex structures created from the circulation around the blades can be expected to occur as described in section 1.3.1. These structures can be illustrated by the λ_2 -method, used in figure 5.14 on instantaneous results from the single wind turbine simulation. One can however not see any dominant trailing vortex structures. The vorticity field is dominated by small structures, mainly originating from the outer half of the blades. It has not been possible to identify any root vortex structures, whereas the tip vortices appear to be scattered. Whether this is a result of not resolving the aerodynamics of the blades or early breakup of vortex structures is a question of high relevance to evaluate the reliability of the results. The scattering might be an effect of the high tip-speed ratio, which decreases the distance between vortices leading to increased interaction and earlier breakup. It is however also possible that

the vortex formation is insufficiently captured due to low resolution in time and space, thereby not contributing to a representative development of the wake downstream. The recirculation concluded in section 5.1 can explain the absence of root vortices since the recirculation will prevent formation and transportation of vortices downstream. The recirculation will both break down the structures and transport the remaining turbulence toward the blade tips.

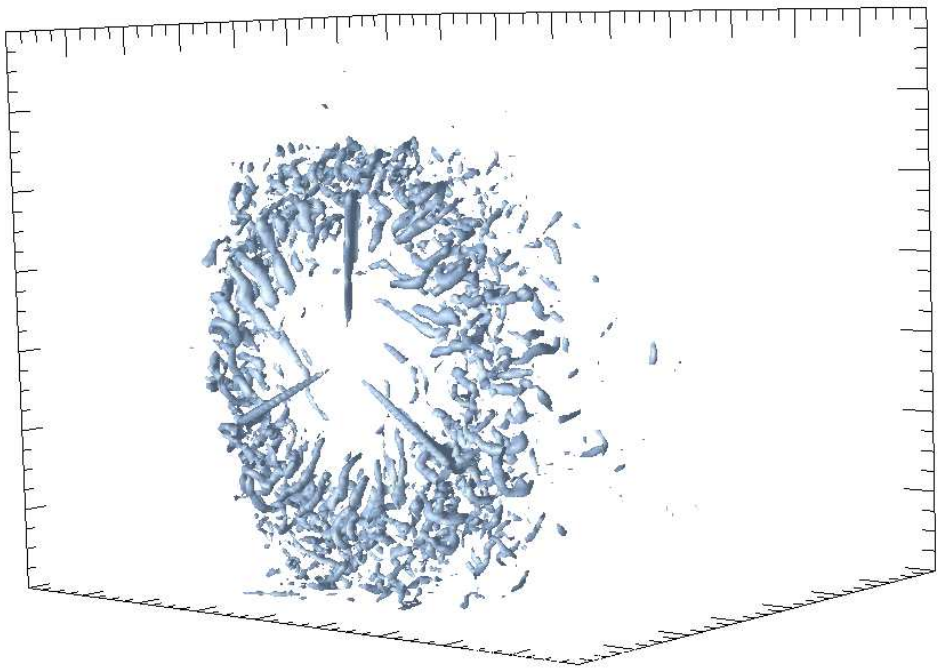

Figure 5.14: Vorticity illustrated by λ_2. Single wind turbine.

In figure 5.16 is the instantaneous axial velocity around one of the blades is illustrated at a cross section 0.4 units from the hub center. The cross section is shown in figure 5.15. The blade is moving toward the bottom of the picture, and it is possible to see that the flow does merely recover to the free-stream flow speed between two blade passages. This is an important factor to explain the heavy recirculation behind the rotor. A particle in the free-stream flow travels about 0.1 units in axial direction between two blade passages. This length can be compared with the chord length of

about 0.03 units at the position in the figure. Since the axial velocity at the rotor plane is lower than the velocity in the undisturbed flow, one can conclude that the chord length and axial travel is in the same order of magnitude. The short axial travel distance between two blade passages does not only explain the recirculation, but is also most likely the reason for the scattered tip-vortices. Adjacent tip-vortices interact close to the point where they are formed. It should be mentioned that the resolution during the computations were twice as high as the resolution of the blade in the picture.

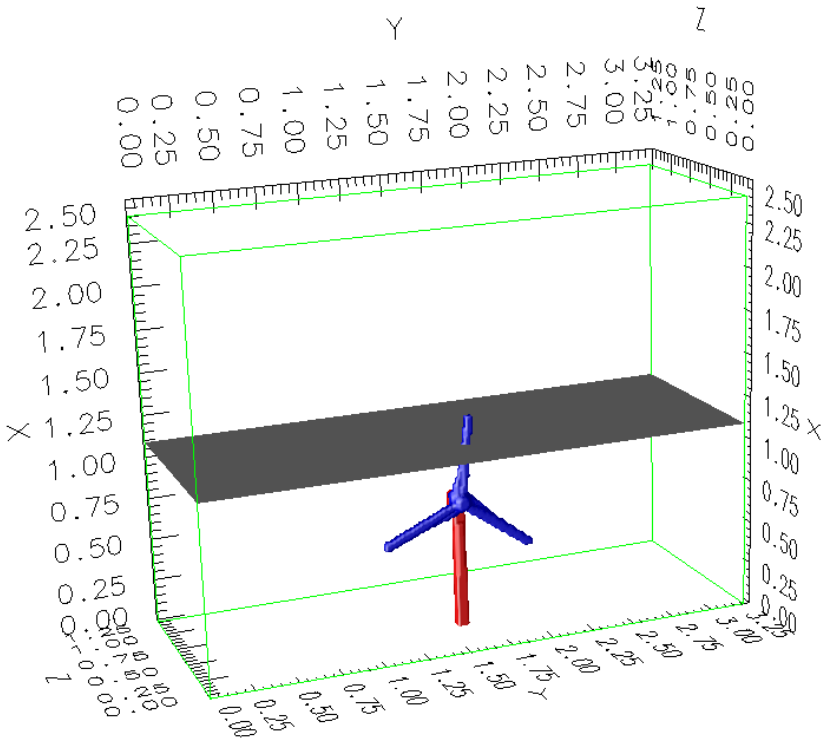

Figure 5.15: Cutting plane used in figure 5.16, 5.17 and 5.18

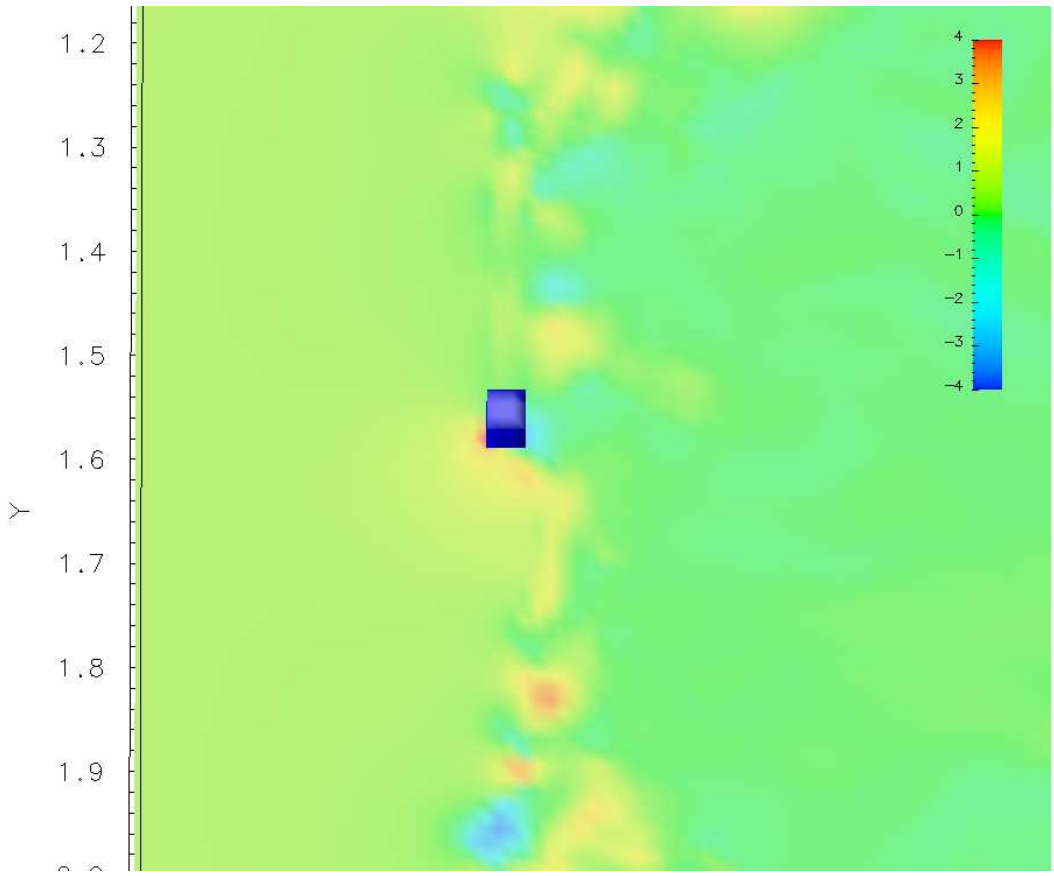

Figure 5.16: Instantaneous velocity in axial direction around one blade at 0.4 units from the hub center. Blade moving towards the bottom of the picture. -0.9°pitch.

The velocity-component in the tangential direction of the blade is illustrated in figure 5.17, and the blade moves toward the bottom of the picture. One can observe that the velocity in negative Y-direction increases significantly behind the trailing edge of the blade. This is expected since the wake should rotate counter-wise the rotor rotation, according to the theory. The magnitude of the velocity indicates a substantial deflection of the flow. It is also possible to observe this structure from the preceding blade passage and conclude that the structures interact between adjacent blade passages. The magnitude and large deflection angle are indications on poor physical representation of the flow around the blade.

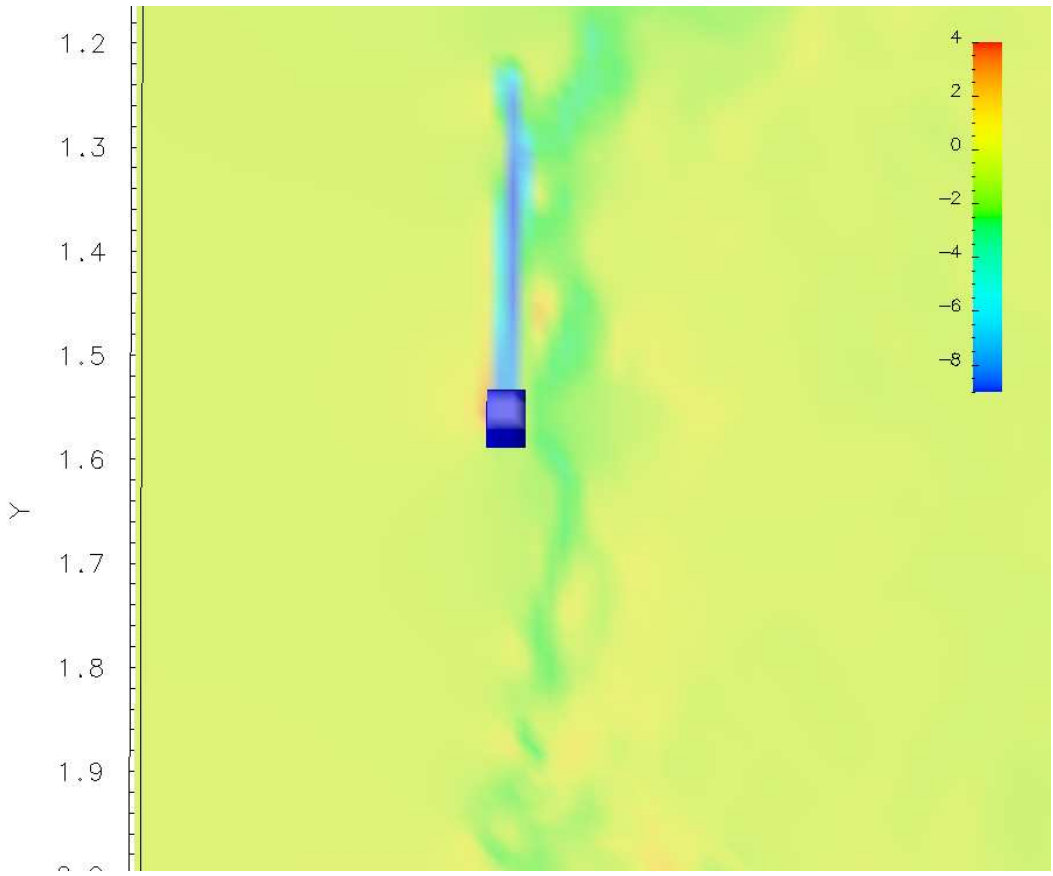

Figure 5.17: Instantaneous velocity in horizontal direction around one blade at 0.4 units from the hub center. Blade moving towards the bottom of the picture. -0.9°pitch.

The large angle of deflection is also illustrated in figure 5.18 showing vectors of the velocities in the plane. The lengths of the vectors indicate a significant acceleration of the flow in negative Y-direction. One can also distinguish the complexity of the recirculation-zone occurring behind the rotor from the figure.
The vectors in the immediate vicinity of the blade show that the flow is detached from the blade. This is an important feature to consider when comparing with the results presented by Edon [10]. These results have been obtained with the assumption of laminar flow, thus attached. Furthermore are the results from the simulations contradictory, showing both a high rate of deflection and detached flow. This is further indications on poor resolution in the vicinity of the blades.

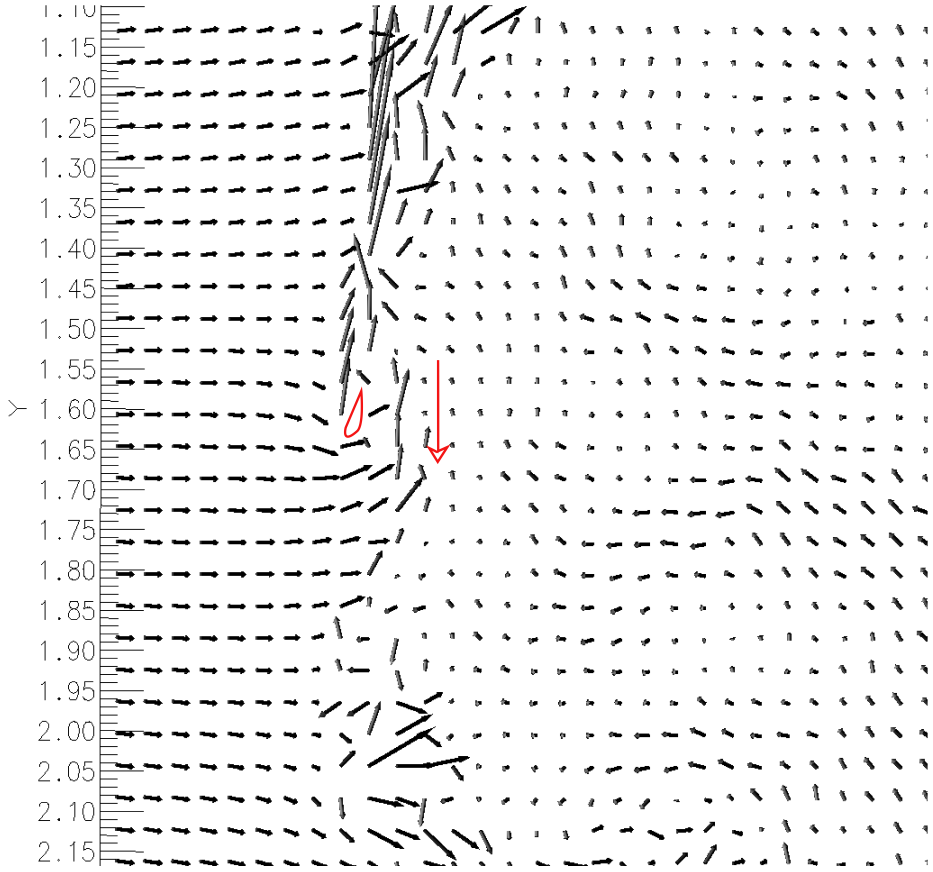

Figure 5.18: Instantaneous vector-field in horizontal direction around one blade at 0.4 units from the hub center. Blade moving towards the bottom of the picture. -0.9°pitch.

5.5 Turbulence resolution

When carrying out LES it is important to verify that the spectrum of turbulence, shown in figure 3.1, is sufficiently captured. Whether it is captured depends both on the resolution in time and space. Figure 5.19 shows the energy spectrum from the simulations, where the normalized energy is plotted as a function of the wavenumber which is normalized with the blade passage frequency. It is possible to conclude that the region with the $-5/3$ inclination is partly captured in the simulations, which implies that the energy containing range is covered. The resolution is thus sufficient in the aspect of resolving the turbulence.

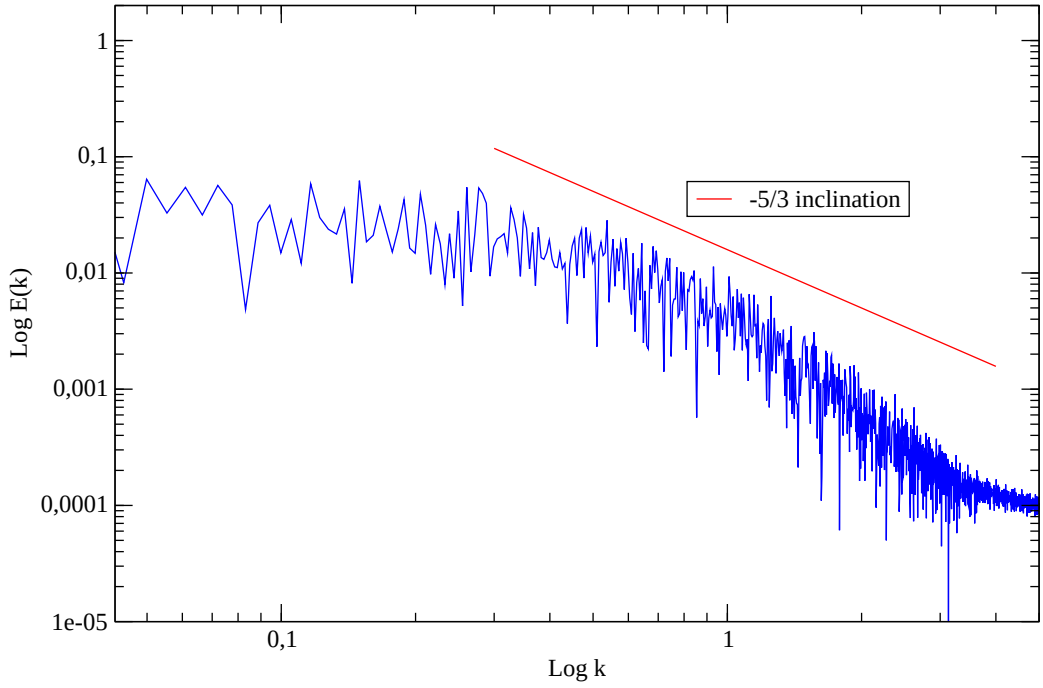

Figure 5.19: Energy spectrum from a point 0.8 units downstream the nacelle of the second wind turbine. Wavenumber k normalized with the blade passage frequency. -0.9°pitch.

5.6 Computational performance

The computational performance associated with the simulations is important to consider when evaluating the results and proposing improvements for continued work. The computational performance does also give an indication on which applications are possible to compute within a certain amount of resources.

The duration of the simulations is illustrated in figure 5.20 where the total duration is divided into the flow development and sampling of results. Since the initial flow field of the domain is not representative of the physics of a real flow, it has to develop. When the flow field has converged, and the variations are no longer dependent on the initial conditions, the sampling of results can start. The computational time was in average 12 h per revolution.

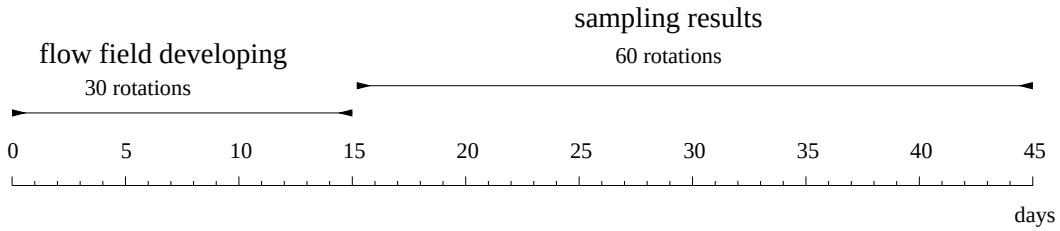

Figure 5.20: Diagram of the duration of the simulations for the cases with two wind turbines.

The computational performance, given in processor-hours, is shown in table 5.1 for cases with one and two wind turbines. It should be emphasized that the figures are approximative estimations since the loading of the computational cluster varies between different runs, affecting the computational duration. The duration can also vary with the time needed to reach converged results within each time-step. It has been possible to identify a small difference in duration between the cases with one and two wind turbines.

Table 5.1: Computational performance

Set-up		Performance	
number of WT	WT distance [units]	number of processors	processor-hours
1	-	5	5,000
2	4.4	10	11,000

Estimations on the computational efforts needed for changes, that might be relevant in future work, is presented in table 5.2. The issue with influence from the boundaries, mentioned in section 5.1 and 5.3, can be treated by increasing the cross section. This can be achieved by a combination of both increasing the number of nodes per domain and increasing the number of domains. In section 5.4 it was concluded that the resolution at the blades might not be sufficient. One method of refinement can be carried out by introducing separate domains for each blade with finer resolution, which rotate along with the blades. This introduces overlapping meshes, and the data has to be interpolated between the blade-domains and the global domain. Another method of refinement is an adaptive refinement, which refines the mesh every time-step along the boundaries of the blade. The influence on the computational

performance is here estimated to be equal, however not verified.
In section 5.3 it was concluded that longer duration of sampling is desirable to further verify and quantify the structures of wake meandering. Longer duration of sampling would also increase the quality and reliability of the results, and might clarify the causes of the asymmetric behaviors. The influence on the computational efforts by duplicating the duration of sampling is presented in table 5.2. Depending on the application of the results and level of reliability desired, even longer durations of sampling might be suggestible.
The increase in processor-hours, and especially the duration, is according to the estimations substantial. This implies that the range of applications is limited with the computational resources available today. The estimations presented are however only rough approximations made by the author, and further studies on alternative methods and implementations has to be carried out in order to provide reliable figures.

Table 5.2: Estimations of computational performance

Set-up			Performance		
number of WT	distance [*units*]	changes	number of processors	processor-hours	duration [*days*]
2	4.4	none	10	11,000	45
2	4.4	doubled cross-section	14	20,000	70
2	4.4	increased resolution along the blades	10-16	18,000	70
2	4.4	increased resolution and doubled cross-section	14-20	27,000	95
2	4.4	doubled sampling duration	10	18,000	75
2	4.4	doubled cross-section and sampling duration	14	33,000	115
2	4.4	increased resolution, doubled cross-section and sampling duration	14-20	45,000	160
2	8.8	doubled distance	10	16,000	50

Chapter 6

Conclusions

A realistic wind turbine geometry has been successfully implemented into the in-house CFD-code developed at the the Division of Fluid-Mechanics. Two main cases were stipulated and set-up, consisting of two wind turbines in a row, with different pitch angles for the first wind turbines. The power extracted by a wind turbine decreases if the pitch angle increases. Since less power is extracted in the case with increased pitch, in theory; more power is left in the flow behind the turbine. This power is available for extraction by the downstream wind turbine, thus distributing the power-extraction more evenly. The real application for this type of control is wind farm optimization and structural load limitations. The geometric changes of pitch angle variation was also concluded to be suitable for studying the sensitivity of the CFD-code.

The CFD-code, employing the virtual boundary method, proved to be able to capture the influence of pitch control by the decreas of power extracted by the first wind turbine. Any significant differences in power extracted by the second wind turbine was not possible to conclude. Initial indications on structures of wake meandering have also been shown. There are however issues compromising the results, implying a need of further development within the treatment of the boundaries of the blades, and most importantly, increased dimensions of the spatial domain.

Quantitative conclusions on the power extraction have not been possible to draw, since no sufficiently accurate method for evaluating it has been possible to utilize. The method used was however concluded to be sufficient for qualitative comparisons between cases. The recirculation behind the wind turbines in the simulations rendered difficulties with the evaluation of the extracted power. This suggests that it might be convenient to implement a tool for evaluating the resultant forces on the

blades, which together with the rotational speed will give the power of the rotor.
It has been possible to investigate the flow field in the near-wake of the wind turbines in the simulations, and conclude that the flow down-stream the blades is both considerably deflected and detached. Consequently there is a contradiction, which indicates poor spatial resolution at the blades. It might also explain the large recirculation zone. In order to verify whether the recirculation is physical or not, simulations of cases with high tip-speed ratio where experimental data is available, should be considered. Higher resolution along the blades is also suggested.
The large expansion of the wake necessitates a larger cross-section, or boundary conditions allowing outflow through the sides and top of the domain. The expansion is connected to the recirculation, and an effect of the back-flow behind the rotor. These characteristics indicates the importance of capturing the 3-D flow along the blades. The conclusion possible to draw, if possible to verify the recirculation characteristics of the simulations with experiments, is that a 2-D airfoil-data representation of the blade characteristics is insufficient for high tip-speed ratio rotors.
The indications of wake meandering are showing that these large scale structures are important features of wind turbine wakes. One can conclude that these structures introduce a need of longer time-duration of sampling, in order to be able to evaluate these structures. Sufficient duration of sampling is also necessary in the sampling of averaged quantities, in order to not introduce an arbitrary unsymmetrical behavior. Furthermore the meandering movements parallel with the rotor plane demands a larger cross-section perpendicular to the main-flow direction. The wake meandering conclusively introduces a substantial amount of computational efforts compared with wakes not showing this feature.
Wake meandering is a large scale phenomenon both in time and space, depending on the geometry of the flow-case. This implies that time-dependent simulations, such as LES, are necessary in order to resolve the structures of a wind turbine wake sufficiently.
The measures of development presented above implies higher computational efforts, not unlikely to more than threefold the computational time needed to carry out the simulations. One can thereby conclude that the method presented is not suitable as a commercial site assessment tool. However, the abilities of full geometry wind turbine simulations, shown in this degree project, indicates that this approach can significantly contribute to a better understanding of wind turbine wakes. This understanding can be useful in more refined characterizations of the commercial wake

models. The method can also be of interest for the development of new rotor geometries, where the computational costs are small compared with full scale experiments. Development within the field of computer performance and code optimization is likely to enhance the full geometry simulations in the long-term view, so is the increased demand of reliable predictions assuring the profitability of future wind farm projects.

Bibliography

[1] Grace. http://plasma-gate.weizmann.ac.il/Grace, (3 February 2011).

[2] Opendx data explorer. http://www.opendx.org, (3 February 2011).

[3] J. Ainslie. Calculating the flowfield in the wake of wind turbines. *Journal of Wind Engineering and Industrial Aerodynamics*, 27(1-3):213–224, 1988.

[4] R. J. Barthelmie, K. Hansen, S. T. Frandsen, O. Rathmann, J. G. Schepers, W. Schlez, J. Phillips, K. Rados, A. Zervos, E. S. Politis, and P. K. Chaviaropoulos. Modelling and measuring flow and wind turbine wakes in large wind farms offshore. *Wind Energy*, 12(5):431–444, July 2009.

[5] F. Bertagnolio, N. Sørensen, J. Johansen, and P. Fuglsang. *Wind turbine airfoil catalogue*. Risø-R. Risø National Laboratory, 2001.

[6] A. Crespo and J. Hernandez. Turbulence characteristics in wind-turbine wakes. *Journal of Wind Engineering and Industrial Aerodynamics*, 61(1):71–85, 1996.

[7] J.-Å. Dahlberg. Vattenfall vindkraft ab. interview, 13.09.2010. Jämtlandsgatan 99 Vällingby, Sweden.

[8] J.-Å. Dahlberg and P. H. Alfredsson. A preliminary wind tunnel study of windmill wake dispersion in various flow conditions. Technical report, The Aeronautical Research Institute of Sweden, 1979.

[9] S. Dixon. *Fluid Mechanics and Thermodynamics of Turbomachinery*. Elsevier Butterworth-Heinemann, 5 edition, 2005.

[10] M. Edon. 38 meter wind turbine blade design - internship report. *Folkecenter for Renewable Energy*, 2007.

[11] T. M. Fletcher and R. E. Brown. Simulation of wind turbine wake interaction using the vorticity transport model. *Wind Energy*, 13(7):587–602, 2010.

[12] S. Ivanell. *Numerical Computations of Wind Turbine Wakes*. PhD thesis, KTH, Stockholm, Jan. 2009.

[13] D. Lörstad. *Numerical modeling of deforming bubble transport related to cavitating hydraulic turbines*. PhD thesis, LTH, Lund, Sweden, 2003.

[14] D. Medici. *Experimental Studies of Wind Turbine Wakes – Power Optimisation and Meandering*. PhD thesis, KTH, S-100 44 Stockholm, Sweden, Dec. 2005.

[15] D. Medici and P. H. Alfredsson. Measurements behind model wind turbines: Further evidence of wake meandering. *WIND ENERGY*, (11), 2008.

[16] M. Ohlsson and L. Fuchs. Significant terms in dynamic sgs-modeling. In P. Voke, L. Kleiser, and J.-P. Chollet, editors, *Direct and Large Eddy Simulations I*. Kluwer Academic Publishers, 1994.

[17] J. Revstedt. *On the Modelling of Turbulent Flow and Mixing in Stirred Reactors*. PhD thesis, LTH, Lund, Sweden, 1999.

[18] S. Schreck. The nrel full-scale wind tunnel experiment introduction to the special issue. *WIND ENERGY*, 5:77–84, 2002.

[19] H. Snel, J. G. Schepers, and B. Montgomerie. The mexico project (model experiments in controlled conditions): The database and first results of data processing and interpretation. *Journal of Physics: Conference Series*, 75(1):012014, 2007.

[20] J. N. Sørensen. Aerodynamic aspects of wind energy conversion. *Annual Review of Fluid Mechanics*, 43(1):427–448, 2011.

[21] J. N. Sørensen and A. Myken. Unsteady actuator disc model for horizontal axis wind turbines. *Journal of Wind Engineering and Industrial Aerodynamics*, 39(1-3):139–149, 1992.

[22] J. N. Sørensen and W. Z. Shen. Numerical modeling of wind turbine wakes. *Journal of Fluids Engineering*, 124(2):393–399, 2002.

[23] R. Szasz and L. Fuchs. Computations of the flow around a wind turbine: Grid sensitivity study and the influence of inlet conditions. *NNFM*, 110, 2010.

[24] H. Tennekes and J. Lumley. *A First Course in Turbulence*. The MIT Press, 1972.

[25] J. Tu, G. H. Yeoh, and C. Liu. *Computational Fluid Dynamics*. Elsevier, 2008.

[26] H. von Renouard and E. Hau. *Wind Turbines Fundamentals, Technologies, Application, Economics*. Springer-Verlag, Berlin Heidelberg, 2 edition, 2006.

[27] F. White. *Fluid mechanics*. McGraw-Hill series in mechanical engineering. McGraw-Hill, 6 edition, 2008.

[28] T. Wizelius. *Vindkraft i teori och praktik*. Studentlitteratur, (in Swedish), 2:3 edition, 2007.

[29] A. Zervos, C. Kjaer, S. Azau, J. Scola, and J. Quesada. Pure power - wind energy targets for 2020 and 2030. Technical report, European Wind Energy Association, Nov. 2009.

Appendix A

Blade parameters

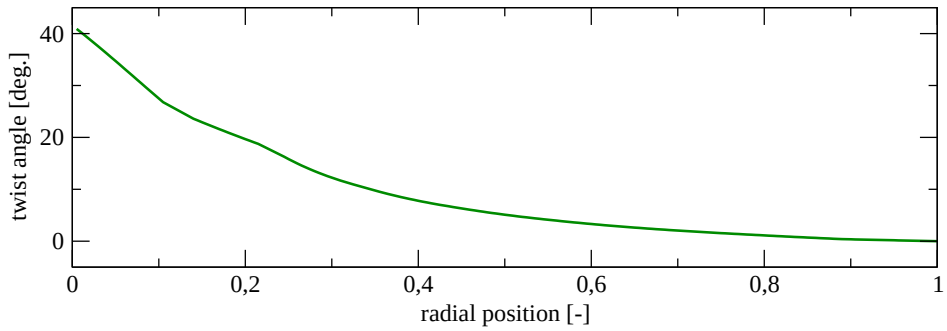

Figure A.1: Twist angle along radial direction after [10] with modifications from radial position 0 - 0.05, fiting the blade to the hub

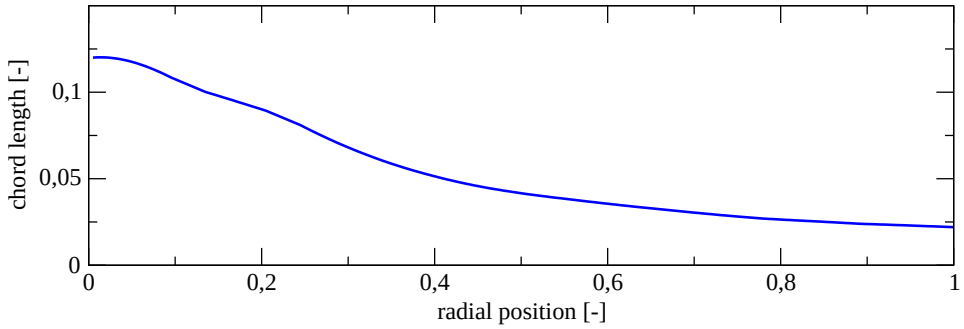

Figure A.2: Chord length along radial direction after [10] with modifications from radial position 0 - 0.05, fiting the blade to the hub

Appendix B

Meandering

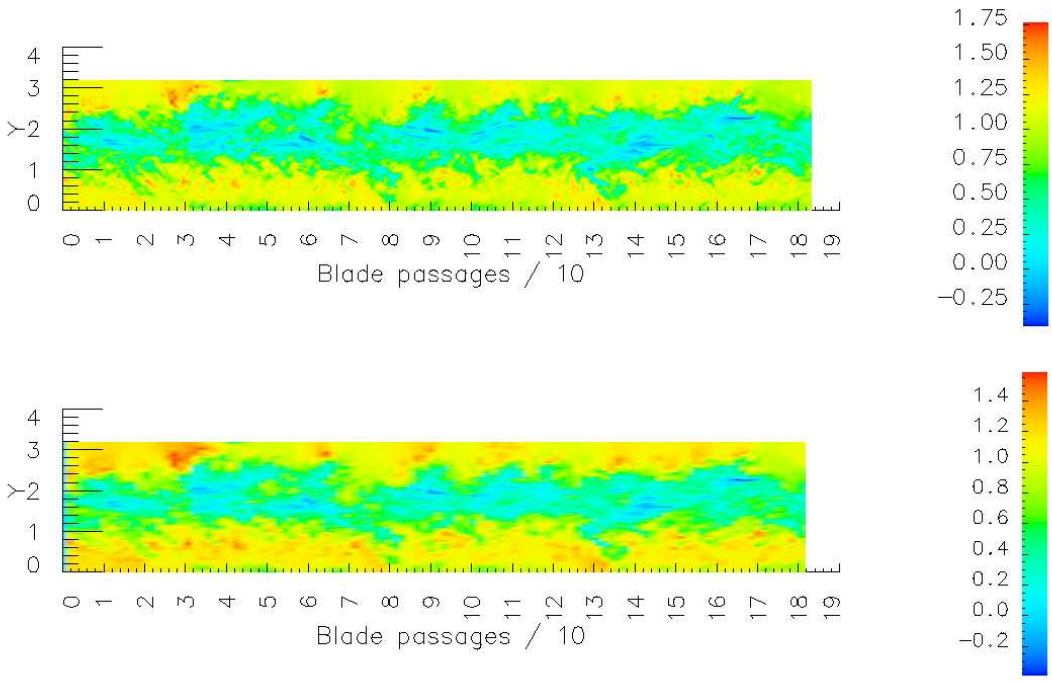

Figure B.1: Axial velocity over time along a horizontal line 4 units behind the first rotor. Filtering carried out by averaging over 1/3 and 5/3 blade passages (from above). -0.9°pitch.

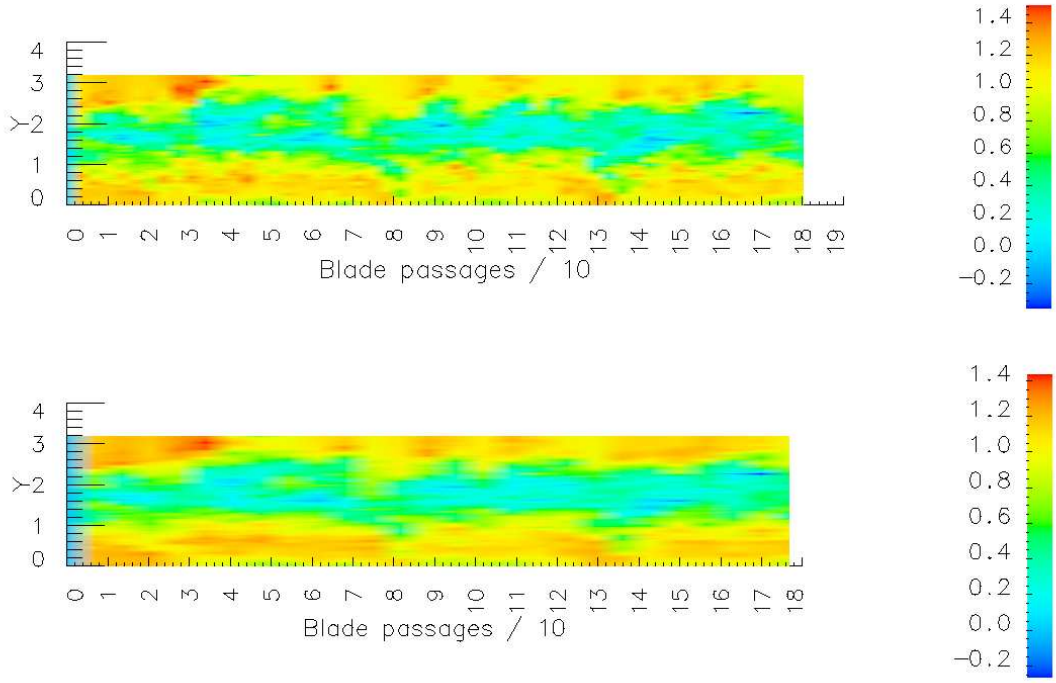

Figure B.2: Axial velocity over time along a horizontal line 4 units behind the first rotor. Filtering carried out by averaging over 10/3 and 20/3 blade passages (from above). -0.9°pitch.